The polymorphic landscape of halogen-bonded cocrystals

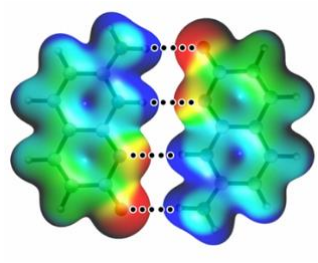

Christelle Hajjar

Thesis Submitted to the University of Ottawa in Partial Fulfilment

of the Requirements for the Degree of Master's in chemistry

Table of contents

Abstract

Cocrystals have attracted much interest in recent years. It was once thought that cocrystals could be a means to prevent polymorphism but many recent examples of cocrystal polymorphism have been discovered and reported. In this contribution, we present a survey of polymorphic cocrystals.

Polymorphism is the ability of a specific chemical compound to crystallize in more than one crystalline form. Polymorphs have different arrangements of the molecules in the given crystal lattice and may exhibit different characteristics such as packing properties, thermodynamic properties, spectroscopic properties, kinetic properties, surface properties, and mechanical properties. Polymorphs can be classified in various groups such as crystalline, amorphous, hydrates, and solvates. The main characterization methods used in this thesis are X-ray diffraction and solid-state NMR spectroscopy.

The concept of variable stoichiometry cocrystallization is explored in halogen-bonded systems. Three novel cocrystals of 1,4-diiodotetrafluorobenzene and 3-nitropyridine with molar ratios of 1:1, 2:1, and 1:2, respectively, are prepared by slow evaporation methods. Powder X-ray diffraction experiments carried out on the 1:1 and 2:1 cocrystals confirm that gentle grinding does not alter the crystal forms.

$^{1}H \rightarrow {}^{13}C$ and $^{19}F \rightarrow {}^{13}C$ cross-polarization magic angle spinning (CP/MAS) NMR experiments performed on powdered samples of the 1:1 and 2:1 cocrystals are used as spectral editing tools to select for either the halogen bond acceptor or donor, respectively.

I also describe the formation of a new cocrystal of 1, 3, 5-trifluoro-2, 4, 6-triiodobenzene and piperazine with a 2:1 molar ratio that was prepared by the slow evaporation method. In addition of that, I have prepared the cocrystal (1,4-

diiodotetrafluorobenzene)(coumarin) already reported. After preparation and purification process of this compound, I obtained a small amount powder, but could not characterize it by solid-state NMR; rather I performed powder X-ray diffraction to study this compound.

Overall, this work contributes new examples to the field of polymorphism in halogen-bonded systems and to variable stoichiometry cocrystal engineering with halogen bonds.

Acknowledgements

I would not finish this work without the help and support of many friends, family, colleagues, and mentors that I've worked with over the past couple years. First and foremost, I would like to thank Professor David L. Bryce, my supervisor, for his exceptional guidance throughout my time in the Bryce Lab. Thank you for your guidance, for having confidence in me, and providing me a lot of advice and suggestions that helped me through my masters.

I would also like to acknowledge Professor Alain St-Amant and Professor Paul Mayer for reading this thesis and providing me valuable comments, and for being in my advisory committee.

To my friends and colleagues at the University of Ottawa – thank you for your thoughtful discussions, for your support as well. Especially, Tamali Nag and Peter Pallister, for helping me doing NMR experiments with calculations. Peter Pallister at the University of Ottawa NMR lab, your advice and technical support was invaluable throughout this work. Jeffrey Ovens for your assistance in doing PXRD and single x-ray experiments. To my fellow Bryce Lab colleagues, I appreciate our collaboration over the years. Glenn Facey, you first introduced me to solid-state NMR through the course you gave in the beginning of my masters, I cannot say how valuable this course was for me. To Tamali Nag, Vincent Morin, Shubha Gunaga, Hashim Al Sayed, Dan Zheng, Dr. Yijue Xu, Dr. Scott Southern and more recent fellow graduate students, life in the office and in the lab would not be as interesting without you.

Finally, I would like to thank all my family and relatives for their love and support, especially my husband. I want to present this work to my sister's and Mom's souls, they passed away this year and they were always supporting me and confident that I will make it. Dad, over the years you've challenged me to go as far as I can in my education, and you always say that I can do it.

Statement of Originality

I certify that the work presented in this thesis is my own work. With permission from the publisher, the scientific contribution of this work is based on my own published work in peer-reviewed journals:

Hajjar, C.; Nag, T.; Al Sayed, H.; Ovens, J.; & Bryce, D. L. Stoichiomorphic Halogen-Bonded Cocrystals. A Case Study of 1,4-Diiodotetrafluorobenzene and 3-Nitropyridine. *Canadian Journal of Chemistry*. **2021**, in press. doi: 10.1139/cjc-2021-0245

Hajjar, C.; Ovens, J.; Bryce, D. L. 1,3,5-Trifluoro-2,4,6-triiodobenzene–piperazine (2/1). *IUCrData*, **2021**, *6*, x211044. https://doi.org/10.1107/S2414314621010440

List of figures

List of tables

Chapter 1: Overview and Objectives

1.1 Overview

It is interesting to explore the stoichiometric landscape for many reasons, including modulation of physicochemical properties, and to improve our understanding of the role stoichiometry plays related to the concepts of polymorphism and solvate formation[1]. Variable stoichiometry cocrystals,or stoichiomorphs, are solid crystalline phases composed of two or more molecular components prepared in different molar or stoichiometric ratios[1]. Generating distinct crystalline phases composed of the same molecular building blocks is an important tool[3].

In this work, I have chosen these halogen bond donors 1 and 3 because they are the commonly used and they are strong halogen bond donors. I have selected 3-nitropyridine, piperazine and coumarin, 2,4 and 5 as shown in **Figure 1**, as halogen bond acceptors because normally the nitrogen atom is one of the most reliable bases for the formation of halogen bonds in general and with perfluorinated iodobenzenes in particular. We describe the results of our efforts to explore the stoichiomorphic landscape of a halogen-bonded cocrystal system. We present the formation of halogen bonded cocrystal prepared from 1,4-diiodotetrafluorobenzene and 3-nitropyridine with various stoichiometric ratios. Halogen bonds are electrophilic non-covalent interactions between an area of elevated electrostatic potential on a halogen atom and an electron donor moiety[3]. In addition, we describe the formation of a novel halogen bonded cocrystal prepared from 1,3,5-trifluoro-2,4,6-triiodobenzene and piperazine. These interactions that have influence on the flexibility of

the crystal structures and offer a unique opportunity in the strength, atom size, and interaction gradation[4,5,6].

The halogen bond donor was chosen in part due to its reliable ability to predictably form one-dimensional halogen bonded chains, while the halogen bond acceptor was explored as a novel electron donor system potentially capable of interacting at nitrogen and/or oxygen sites, thus increasing the potential for polymorphism and stoichiomorphism[5].

Furthermore, the low melting point of 3-nitropyridine (35-40°C) means that cocrystallization could potentially provide a route to stabilizing this component in a higher-melting solid phase. In addition, we present an example of cocrystal of coumarin and 1,4-diiodotetrafluorobenzene and employ powder X-ray diffraction methods for the characterization of the cocrystals. We also demonstrate the value of $^{1}H \rightarrow {}^{13}C$ and $^{19}F \rightarrow {}^{13}C$ cross-polarization magic angle spinning (CP/MAS) NMR experiments both to confirm cocrystal formation in powdered samples and for spectral editing purposes [8,9,10].

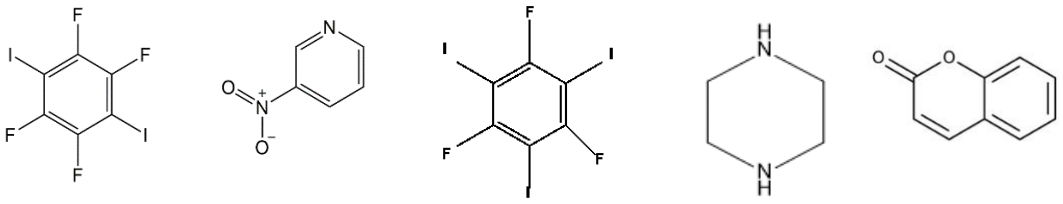

1 2 3 4 5

Figure 1. Molecular structures of halogen bond donors **1** (1,4-diiodotetrafluorobenzene) and **3** (1,3,5-trifluoro-2,4,6-triiodobenzene), halogen bond acceptors **2** (3-nitropyridine), **4** (piperazine), and **5** (coumarin).

Chapter 2 is an introduction to crystal structures and polymorphism. It contains the definition of polymorphism, the preparation methods used for polymorphs. and the characterization methods (powder X-ray diffraction, single crystal X-ray diffraction, solid-state NMR spectroscopy) used in this these to study polymorphs.

In chapter 3, we describe non-covalent interactions, halogen bonding, and we explain the σ-hole theory and provide some historical perspective.

Table 1. List of compounds used.

Compounds	**Abbreviations**
1,4-diiodotetrafluorobenzene	1
3-nitropyridine	2
1,3,5-trifluoro-2,4,6-triiodobenzene	3
Piperazine	4
Coumarin	5

In chapter 4, I describe a literature review using the Cambridge Structural Database and summarize some known polymorphs in halogen bonded cocrystals and their crystal structures. Some attempts to reproduce these polymorphs are described.

In chapter 5 are listed the experimental procedures, including the main results along with a discussion and interpretation. Chapter 6 provides some general conclusions.

1.2 Objectives

The major goal of this thesis is to explore the polymorphic landscape of halogen-bonded cocrystals using different co-crystallization methods and to apply advanced diffraction and NMR characterization methods**.**

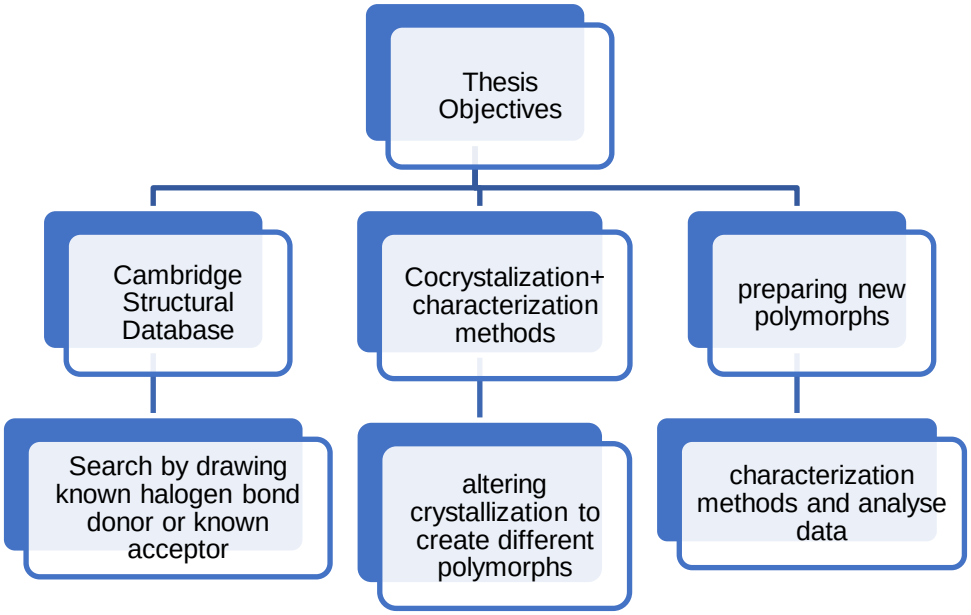

Figure 2. Diagram showing thesis objectives.

The first objective , as shown in **Figure 2**, is searching the Cambridge Structural Database for examples of known polymorphs of halogen-bonded cocrystals , to explore different ways to prepare new polymorphs and to identify good candidates for new polymorphs. The database (CSD) is the world's repository for small-molecule organic and metal-organic crystal structures.

The second objective to repeat some co-crystallization examples from recent papers and characterize them via different methods (^{13}C solid-state NMR,melting point,powder X-ray, and single-crystal X-ray diffraction).Then, after repeating some co-crystallization

examples, I have tried altering crystallization conditions to generate new and different polymorphs.

Table 2 shows the halogen-bonded polymorphs I found by searching the Cambridge Structural Database, and their structures, space groups, and formulas.

Table 2. Some examples of polymorphs in halogen-bonded solids.

Pairs	polymorph	Structure	Space group	Formula
A	1	JUZRED	P 1(2)	$C_{18}H_{15}OP$, 2(C_6 F_4 I_2)
	2	JUZRUT	P 21/c	
B	3	JUZRON	P1 (2)	C_{18} H_{15} O P, C_6 F_3 I_3
	4	JUZRON 01	P21/c	
C	5	ANUQAC	P21/c	C_{18} H_{15} O P, C_6 F_4 I_2
	6	LEJBUA	P 1 (2)	6(C_{18} H_{15} O P),5(C_6 F_4 I_2)
D	7	VUYPUC	P2/c	C_{14} H_8 Cl_2 N_2
	8	VUYPUC01	P b c a	
E	9	XAYLOB	P21 /n	C_{14} H_8 N_2, C_6 F_3 I_3
	10	XAYLUH	P21/c	
F	11	QODPOR	P21/c	2(C_9 H_6 O_2), C_6 F_4 I_2
	12	QODPOR01	C 2/c	
G	13	QEWWIB	P1 (2)	(C_{19} H_{18} P) $^+$ I_3 $^-$. (C_6 F_4 I_2)
	14	QEWWOH	P21 /n	
H	15	QEWWUN	P2/c	(C_{19} H_{18} P) $^+$ (I_3) $^-$.2(C_6 F_4 I_2)
	16	QEWXAU	Pbca	2(C_{19} H_{18} P) $^+$ 2 (I_3)$^-$.3(C_6 F_4 I_2)

Chapter 2: Introduction to crystal structures and polymorphism

2.1 Introduction

Molecular and ionic solids can adopt a range of forms depending on how they are prepared [1,11]. Such forms include pure crystalline (ex: Na^+Cl^-) or amorphous phases (ex: glass), hydrates, or solvates (ex: unit cell of the theophylline DMSO) (**Figure 4**). In bicomponent or multi-component molecular system, it is often possible to form cocrystals as well as hydrates or solvates of cocrystals. Cocrystals are defined as solids that are crystalline materials composed of two or more molecules in the crystal lattice. Other definitions refer to a definite stoichiometric ratio of the constituent molecules. Cocrystal engineering is a topic of broad interest with many applications[1,11].

Polymorphism refers to the ability of a molecule to crystallize in more than one crystal lattice – i.e., the ability of the same pure chemical components to have different crystal structures [12]. Polymorphism was first discovered in 1821 by the German chemist Eilhard Mitscherlich and it is a very commonly known phenomenon in the pharmaceutical world which exhibits in crystalline materials [13]. The importance of all these variations (amorphous vs crystalline, hydrates and solvates vs anhydrous forms, and polymorphism) is by now well known, with particular interest from the pharmaceutical industry due to the differences in physicochemical properties of different forms, and the associated intellectual property concerns.

Pseudopolymorphs are often studied alongside polymorphs. This term typically refers to hydrates or solvates of crystal phases (**Figure 3**).

The first cocrystals reported were the cocrystals of hydroquinone and quinone in 1844 by Friedrich Wöhle. Co-crystals directly affect the solid-state properties in terms of solubility and bioavailability[13].

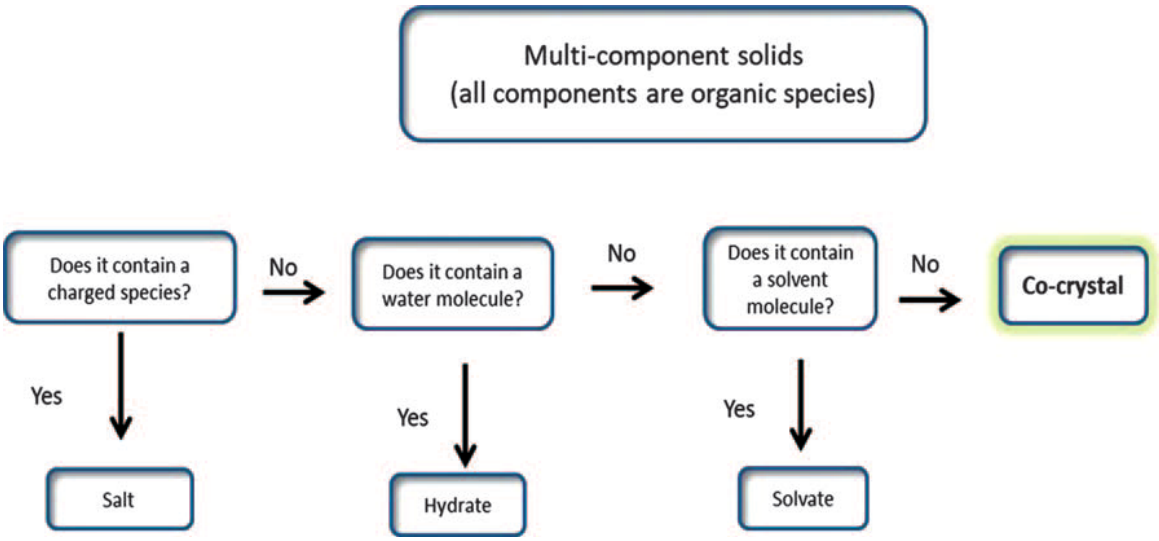

Figure 3. Simplified flowchart for classifying organic multi-component solids. Reprinted with permission from reference 1 (Aakeröy & Sinha, 2018)

2.2 Polymorphism types

2.2.1 Enantiotropic systems

When one polymorphic form changes to another at a fixed temperature (transition temperature) reversibly the phenomenon is called as enantiotropy and the polymorphic forms are said to be enantiotropes of each other. The transition temperature is always less than the melting point of either polymorph; if not, no phase transition will be detected [13].

2.2.2 Monotropic systems

Monotropic systems are those where when one polymorphic form is stable at all the temperatures below its melting point and all other forms are metastable. This is referred to as monotropy and the two polymorphs are said to be monotropes of each other. The metastable form changes to the stable form at all temperatures and the change is not reversible. As a result, all other metastable polymorphs have no region of stability anywhere on a pressure-temperature diagram [13].

2.3 Types of polymorphs

2.3.1 Crystalline form

Two crystalline polymorphs have a different arrangement of the molecules in the crystal lattice. Crystalline solids are usually highly stable and have well-established properties. Most of the drugs used have a crystalline form[13].

2.3.2 Amorphous form

This type of form consists of arrangements of molecules randomly placed with a high degree of disorder in the given space; it is also called a non-crystalline solid form. The amorphous state is usually much faster dissolving than the crystalline form and has a variable solubility that is usually higher than the crystalline form. The amorphous form is often less stable than the crystalline form and is usually hygroscopic in nature.[13].

2.3.3 Solvate form

When crystal forms contain either stoichiometric or non-stoichiometric amounts of a solvent within the crystal lattice, they are referred to as solvates. If the incorporated solvent is water, the solvate is called a hydrate. Depending on the number of molecules of water incorporated, this crystal is called as the monohydrate, dihydrate, trihydrate, etc. Hydrates are the most observed class of solvates. Besides water, residual solvents used in the process can be incorporated and form solvates [13].

2.3.4 Cocrystal

Cocrystals are formed from crystalline materials which composed of two or more different molecules, in the same crystal lattice. These are bonded with each other through non-covalent bonding such as hydrogen bonding, halogen bonding, van-der-Waals interactions, or π-interactions, for example. These materials are designed through crystal engineering for better solubility and stability of drug molecules [14]. Cocrystals are attractive because the cocrystal solid can be designed to have superior physical properties than either of the pure starting molecules[15].

As cocrystal research has expanded, it has available a range of application areas for physical property manipulation through cocrystal formation. Improvements in solubility, stability, bioavailability, and mechanical properties have been well documented, and emerging applications such as taste masking and intellectual property extension are being explored. [15,16].

Research in cocrystal structure and applications has shown an exponential increase in the past decade, evident in the number of cocrystal structures deposited in the Cambridge Structural Database and cocrystal related patent applications.

Considering this, it is surprising that cocrystal preparation methods have remained, until relatively recently, largely poorly defined. Limited research attention has been directed specifically at cocrystal preparation, and this topic receives little detail in most existing publications. Initial cocrystal related research efforts centered on elucidation of the crystal structure of cocrystal and bonding mechanisms, requiring high quality single crystals from cocrystal samples.[15]

Solution based cocrystallization routes were employed, requiring knowledge of the solubility of both starting materials in the solvent of choice, often supplied in the format of a ternary phase diagram. Again, methods used were inconsistent from research paper to research paper, and no universal approach was practiced.

Today, a wide range of successful cocrystal preparation methods have been documented: solvent evaporation, solid state grinding, solution crystallization, slurry conversion, melt crystallization, hot melt extrusion, and spray crystallization[15].

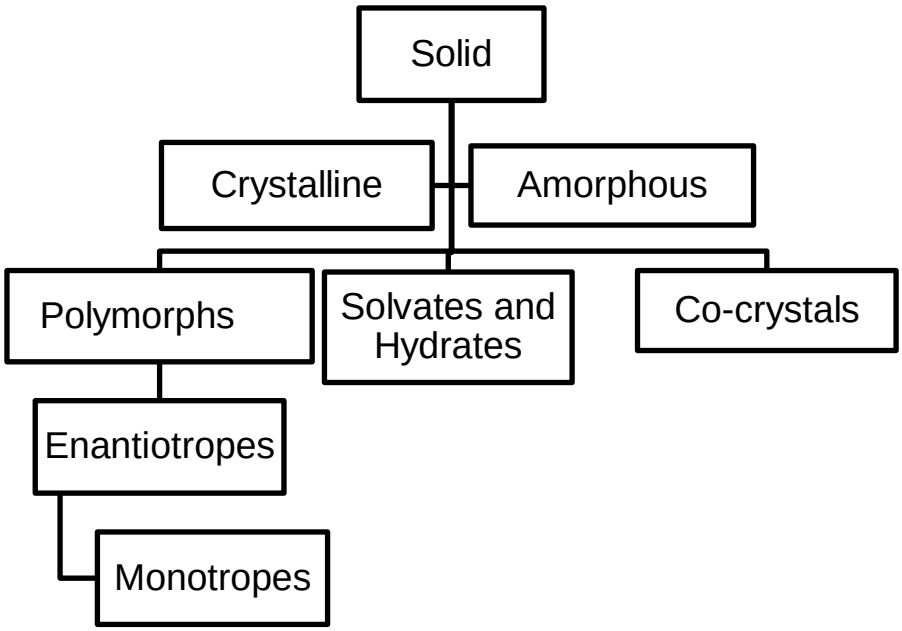

Figure 4. Classification of solids. Reprinted from reference 14 (Gosar et al., 2019).

2.4 Screening of polymorphs of cocrystals

Despite the few reports aimed specifically at polymorph screening of cocrystals, they provide useful reference on the different methods for cocrystal polymorph screening. Therefore, we highlight here some of the significant contributions on the topic.

Crystallization from solution is the most common method for polymorph screening because it generally yields single crystals that can be analyzed by single crystal X-ray diffraction. The wide range of experimental conditions during solution crystallization may improve the chances of identifying new polymorphs. For example, cocrystallization experiments can be conducted from solvents of different polarities and solvent mixtures. The rate of evaporation of the solvent can also be varied by changing the experimental temperature. A few recent polymorphs of cocrystals have been obtained by conventional crystallization experiments[15].

2.5 Physical properties of crystal forms.

The different arrangement creates a difference in the energies of two polymorphs, as the changes in their physical properties such as mechanical properties and packing properties, **(Table 3)**. The polymorphism can affect the quality, safety, and efficacy of a compound[14].

Table 3. Physical properties of different crystal forms. Adapted from reference 14 (Gosar et al., 2019).

Property type	**Example**
Thermodynamic	Melting point, solubility, entropy
Spectroscopic	Electronic, vibrational, and nuclear spin transitions
Packing	Refractive index, density, and Molar volume,
Kinetic	Dissolution rate, rate of reaction and stability
Surface	Surface free energy, crystal habit, interfacial tensions
Mechanical	Hardness, compactibility, flow and blending

2.6 Methods of preparation of polymorphs

Many new methods have been investigated to induce the polymorphic transitions and this section will discuss a few most employed ones in brief[13].

2.6.1 Solvent evaporation method

In this approach, the saturated solution of the drug is prepared in an appropriate solvent and the solvent is removed by rotatory evaporation. Air drying at various temperatures, can also be employed to obtain different potential polymorphs[13].

2.6.2 Slow cooling approach

This technique is frequently employed for the polymorphic forms in the solvent systems having boiling point range of 30 to 90°C. In brief, the solute is heated in the solvent just above the boiling point of the latter to produce the saturated solution. This solution is transferred to a stoppered tube and is connected to a Dewar flask containing water at a temperature just below the boiling point of the solvent. The Dewar flask is left in these conditions for several days. Variation in the solvent composition may inhibit or promote growth of crystal faces and hence, can yield crystals of the desired morphology. This approach is also called the solution growth approach[13].

2.6.3 Solvent diffusion technique

The solution is placed in a sample tube; subsequently, a less dense solvent is carefully dripped down the sides of the tube using either a pipette or a syringe to form a discrete layer. The most employed solvent combination is CH_2Cl_2/ethanol, and this is preferred one, provided the sample is insoluble in ether.

2.6.4 Vapor diffusion method

In this case, the concentrated drug solution is placed as a drop hanging on the underside of a microscope cover slip. The cover slip with the hanging drop is sealed with silicon oil over a solution containing high concentration of precipitant. Due to higher precipitant concentration, the latter has lower vapor pressure than the drug solution. This results in diffusion of the solvent from the drop towards the reservoir and subsequent crystallization within hours to weeks[13].

2.6.5 Vacuum sublimation

Sublimation is known to offer excellent crystals for a variety of compounds, especially the air sensitive ones. This approach is frequently employed to induce crystallization with numerous variations of static or dynamic vacuum. A small amount of sample sealed under vacuum in a reactor is generally subject to a temperature gradient in numerous manners. Temperature of the order of 250°C can be easily employed at a pressure of around 10-2 mm of Hg. The crystals grow from the wall to the center of the reactor. Crystal engineering and supramolecular synthesis (cocrystallization) are being used to enhance solubility, bioavailability, safety, and efficacy of various APIs[13].

2.7 Evaluation Techniques

2.7.1 Dissolution study and Van't Hoff Plot

This study is generally performed in a suitable dissolution medium, generally phosphate buffer saline, pH 7.4. The time dependent solubility studies are presented, and the dissolution profile of various polymorphs is compared. The dissolution pattern can be

correlated with the enthalpies of fusion and melting point. The Van't Hoff plot is an important approach to determine the values of dissolution enthalpy (ΔH) and dissolution entropy (ΔS), as per equation 1:

$$(\ln solubility) = -(\triangle \mathrm{H}/\mathrm{RT}) + (\triangle \mathrm{S}/\mathrm{R}) \qquad \textbf{eq.1}$$

For the same, saturated solubilities at least three temperatures are determined and graph between logarithm of molar solubility and inverse of absolute temperature is plotted[13].

2.8 Methods of characterization of polymorphs

Various techniques have been used to characterize the polymorphs like infrared (Fourier Transform Infrared (FT-IR)) spectroscopy, powder X-ray diffraction (XRD), single crystal XRD and solid-state NMR spectroscopy.

2.8.1 Fourier Transform Infrared (FT-IR) Spectroscopy

FT-IR helps to identify the polymorphs by indicating changes in frequencies, relative intensities, band contours, and the number of bands. Difference in spectra gives an inference to the internal arrangement of crystals.

2.8.2 Powder X-ray diffraction (XRD)

XRD is a widely employed and reliable technique to identify different crystal phases through different diffraction patterns. This technique is used for characterizing pharmaceutical solids include the analysis of single crystals and powders. It is based on Bragg equation ($n \lambda = 2 d \sin \theta$) which describes the diffraction of a monochromatic X-ray beam impinging on a plane of atoms. The parallel incident rays beat the crystal planes at an angle θ and are then diffracted at the same angle θ.

The intensities of diffracted rays were determined by the types of atoms present in solid and their rearrangement within a crystalline material. The angle θ is determined by slowly rotating the sample and measuring the angle of the incident beam.

XRD is the analysis of a powder sample with typical output being a plot of intensity versus the diffraction angle (2θ). This type of plot can be considered a fingerprint of the crystal structure and useful for determining the crystallographic similarity of samples by pattern comparison. A peak will be displayed for all repeating planes with the same spacing. An amorphous sample will exhibit a broad hump in the pattern.

Changes in the XRD pattern may be new peaks, shoulders, or a shift providing proof of polymorphic transitions. By comparing the simulated pattern and the experimental pattern of a cocrystal, extra peaks in experimental patterns means impurities however extra peaks in simulated pattern could mean lower symmetry. Also, sometimes peaks are too weak to be able to see it in experimental pattern of powder X-ray. In addition of that, the preferred orientation effects makes some peaks disappear if my sample is large or unground crystals[13].

2.8.3 Single crystal XRD

X-ray diffraction is known as a rapid, non-destructive analysis of multicomponent mixtures without the need for extensive sample preparation. It is used to analyze unknown materials and is useful for characterization in several different fields of research (mineralogy, forensic science, and the biological and pharmaceutical sciences).

Using X-ray diffraction, series information can be obtained, such as the phase identification, crystallinity, lattice parameters, crystal structure refinement and determination, size, and strain broadening, and periodically arranged clusters [13].

2.9 Nuclear Magnetic Resonance Spectroscopy

2.9.1 The Zeeman Interaction

It is useful to begin the discussion of nuclear magnetic resonance (NMR) by first discussing the basics of quantum mechanics. Nuclei possess a nuclear spin quantum number, *I*, which can take the values of integers and half integers of 0, ½, 1, etc., increasing in intervals of one half. Nuclei possessing spin with integer values of *I* are known as bosons while nuclei with half-integer spin values are called fermions[16].

Related to spin is the property called angular momentum, L, given by equation 2 as:

$$L=\hbar(I(I+1)) \qquad \textbf{eq. 2}$$

The nuclear spin angular momentum is a vector with a component along the z-axis. The z-component interacts directly with the applied magnetic field, B_0 (reported in units of

Tesla (T)), which also lies along the z-axis. It is for this reason that the angular momentum operator representing its z-component can therefore be defined by $\hat{I}_Z$.

The angular momentum gives rise to an intrinsic property called the magnetic moment, μ, representing the interaction between the nucleus and the magnetic field. μ is dependent on both the nuclear spin angular momentum and the gyromagnetic ratio, γ (rad s^{-1} T^{-1}). The total energy from this interaction is given by:

$$\mathrm{E} = -\mu B_0 \qquad \textbf{eq.3}$$

The spin quantum number, *I*, has corresponding eigenvalues of m_I, equal to $-I$ to $+I$ in intervals of 1/2. Thus, for any value of *I*, there are precisely $(2I+1)$ eigenvalues.

$$\hat{I}_Z \psi_m = m_1 \hbar \psi_m \qquad \textbf{eq.4}$$

It is now useful to define the Hamiltonian for a spin in a magnetic field. The Hamiltonian operator is dependent on the gyromagnetic ratio, B_0, and the angular momentum operator. Eqn. 5 describes the Hamiltonian:

$$\hat{H} = -\gamma B_0 \hat{I}_z \qquad \textbf{eq.5}$$

The energy, E_m (in units of Joules) representing the eigenstates of the nuclear spin in the presence of the magnetic field is given by eqn. 6:

$$E = -m_l \hbar \gamma B_0 \qquad \textbf{eq.6}$$

Each energy state can be labelled as an α state or a β state, representing the lower energy and higher energy levels, respectively. The transition energy corresponds to the energy which must be subjected to a nuclear spin to induce a transition from the α state to the corresponding β state, matching to a specific electromagnetic frequency. This is referred to as the NMR transition, and the transition typically only occurs when the difference between both values of *m* is equal to exactly one[16,18] .

The frequency of the photon that will induce an NMR transition, or the Zeeman effect is given in eqn. 7, where ν_0 is the Larmor frequency, and is isotopically specific due to its dependence on the gyromagnetic ratio.

$$\nu_0 = \frac{\gamma B_0}{2\pi} \qquad \textbf{eq.7}$$

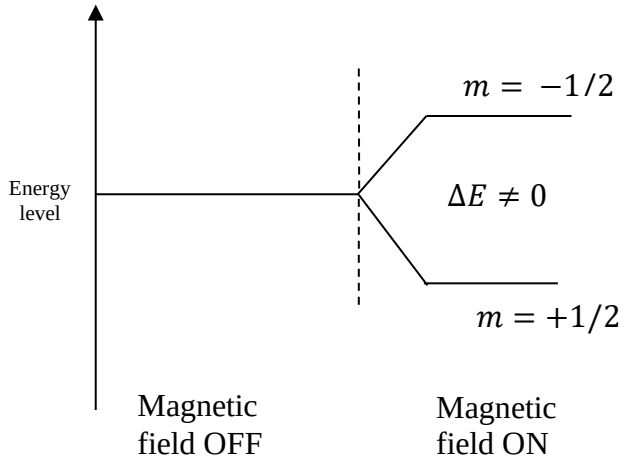

Figure 5. The Zeeman Effect for a spin a ½ nuclide. The splitting of the spin states is observed as a function of the strength of the magnetic field. Reprinted from reference 16 (Levitt, 2008).

In the absence of a magnetic field, the distribution of directions of the spins is isotropic. When a sample is placed in B_0, the interaction of the spin nuclear magnetic moments with the magnetic field will cause their bulk alignment with B_0. This is a process that is time dependent and is characterized by a time constant, T_1, known as the spin-lattice relaxation time constant. The net equilibrium magnetization can be represented by the vector, $\vec{M}$.

The NMR experiment is therefore the practice of manipulating the magnetization vector through space. A sample is placed in a coil which is situated in the xy-plane perpendicular to B_0. By applying a radiofrequency (RF) pulse along the x- or y- axis, the magnetization may be tilted away from the z-axis. In doing so, the magnetization processes around the z-axis at the Larmor frequency, resulting in a component of the vector oscillating in the xy plane.

The vector oscillations can be detected as it induces a current in the coil. These oscillations are detected by the spectrometer. The magnetization vector continues to process around the z-axis, but the cone eventually returns to the thermal equilibrium along the z-axis, causing a gradual decrease of the xy component of the magnetization over time. The detected current in the coil resulting from the oscillations in the xy-plane is known as the free induction decay (FID). The FID is transformed from the time domain to the frequency domain through Fourier transform to an NMR spectrum[16,17,18] .

As it was mentioned before, nuclear spins are affected by their chemical environments. For example, the effects of electronic shielding of the interaction between the nucleus and B_0 would have a direct effect on the resulting NMR transition. Other effects, such as spin-spin coupling, or the quadrupolar interaction of some nuclides can have a major impact on

the NMR spectrum. These NMR interactions are essentially perturbations to the Zeeman interaction. Thus, the NMR spectrum is complicated by the fact that these interactions exist. The Hamiltonian for a spin in a magnetic field is therefore not only dependent on the Zeeman Hamiltonian alone.

In fact, it is additionally dependent on the magnetic shielding interaction, the direct and indirect dipolar coupling interactions, and the quadrupolar interaction in the case of nuclides with spin greater than 1/2. It is therefore essential to examine some of these interactions in detail. For the purposes of this thesis, only the magnetic shielding interaction as well as the indirect spin-spin J-coupling interactions will be discussed in detail[18,19] .

2.9.2 Magnetic Shielding

Magnetic shielding is brought about by the magnetic fields generated by the electrons. These fields may be additive or subtractive to B_0, and consequently change the way the nuclear magnetic moment interacts with the magnetic field.

The magnetic field seen by the nucleus because of the effects of magnetic shielding is given by:

$$B_\sigma = (1-\sigma)\, B_0 \qquad \textbf{eq.8}$$

where σ is the shielding constant.

2.9.3 Spin-spin coupling

In general, coupling results from the interaction between two different spins. Indirect spin-spin coupling (J-coupling) occurs when the interaction between two nuclear spins is mediated by the electrons involved in their bonding. J coupling is typically only a very

small perturbation to the Zeeman interaction. Therefore, it is likely that the other NMR interactions overshadow the presence of this interaction because it tends to be on the order of a few Hz for first-row elements.

Nevertheless, J-coupling is a very important tool for probing the connectivity of atoms in a molecule. In units of Hz, the J-coupling operator between nucleus 1 and 2 is:

$$\hat{H} = 2\pi \hat{I}_1 J \hat{I}_2 \qquad \textbf{eq.9}$$

In the preceding Hamiltonian, J is the orientation-dependent J-coupling tensor. The isotropic J-coupling (J_{iso}) is the average of the principal components of the tensor. The anisotropic contribution to J-coupling (ΔJ) is averaged out in the molecular tumbling of an isotropic solution. However, in the solid state, it remains present, albeit often small. The sign of J_{iso} is dependent on the gyromagnetic ratios of each of the spins for the case of single bonds.

Ramsey's theory states that there are precisely five mechanisms that contribute to the total J-coupling. Fermi contact (FC) is typically the dominant contribution to J-coupling. It is important to recall that s-orbitals have electron density at the nucleus.

The FC contribution arises due to the interaction of the electronic spins and the nuclear spins when the electronic density is at the nucleus. Therefore, the FC contribution is typically a good indicator of chemical bonding. The paramagnetic spin orbit (PSO) and the diamagnetic spin orbital (DSO) mechanisms emerge due to the coupling of angular momenta of the electrons around two nuclear spins. The spin dipole (SD) term is simply

due to the coupling between the nuclear and the electronic spins. Finally, there exists a (FC×SD) cross term which is usually a major contribution ΔJ. It is important to note that the FC mechanism does not contribute to ΔJ [16,18].

2.9.4 Other NMR interactions

Other contributions to the total nuclear spin Hamiltonian which arise due to the interaction with a magnetic field are dipolar coupling and quadrupolar coupling. Direct dipolar coupling is a case of nuclear spin coupling, but in this case, it is a result of the interaction of the two magnetic dipoles resulting from the magnetic moments of each of the nuclei.

It is a through space interaction, as opposed to J-coupling, which is a through-bond interaction mediated by interceding electrons. Accordingly, dipolar coupling can be used to measure the distance between nuclei or give global snapshots of macromolecules. The quadrupolar interaction affects nuclei that have spin greater than 1/2.

The quadrupolar interaction arises because these nuclei have a non-spherical distribution of charge within the nucleus. This distribution is expressed as the quadrupole moment, Q, which couples with the electric field gradient (EFG) caused by the nuclei and electrons within the molecule. This interaction is often very strong, so the quadrupolar interaction usually dominates the NMR spectra of quadrupolar nuclides.

Using all the preceding NMR interactions, it possible to obtain a substantial amount of information about the electronic and molecular structure of a molecule. This is the power of solid-state NMR spectroscopy; it is a tool that has the potential to reveal a lot of information that can lead to conclusions about the nature of molecular systems. In this

work, solid state NMR is used to reveal the nature of noncovalent chemical bonding between atoms[18].

2.10 Experimental Methodology of SSNMR

2.10.1 Magic Angle Spinning MAS

Magic angle spinning (MAS) NMR of solids consists of rapid rotation of the sample about an axis set at 54.7356º relative to *B*o (**Figure 6**). The rotational velocity should be greater than the static (non-spinning) line width.

For ^{13}C and B_o = 9.4 T, typical rotation rates are about 10 kHz, i.e., 600,000 rpm. At these high rotation rates, the strength of the sample holder (the rotor) is critical, with zirconia a common material.

To further reduce stress, the maximum diameter of the rotor is often reduced to 5 mm or less. The drive mechanism is compressed air, and compressed air is also used for all the bearing surfaces. Failure of the bearing air supply is very likely to cause destruction of the zirconia rotor and perhaps the rest of the MAS probe[19].

When the MAS experiment is applied to S=1/2 nuclei such as ^{13}C, ^{29}Si, and ^{31}P, advantage is taken of the ^{1}H spin system, assuming the sample also contains abundant ^{1}H sites.

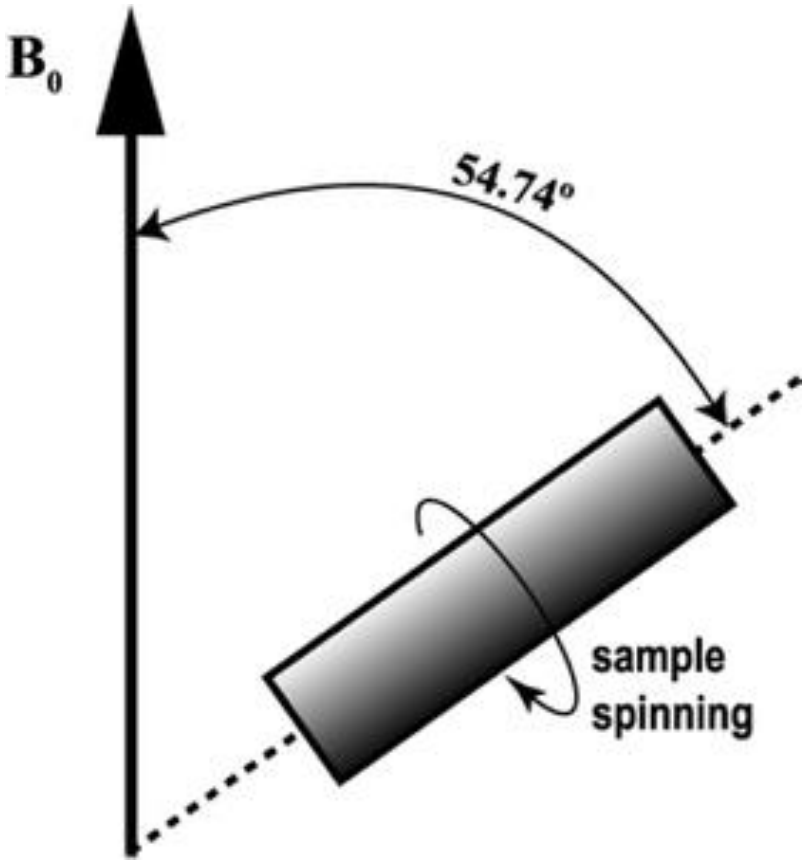

Figure 6. The rapid rotation of the sample around the magic-angle. Reprinted with permission from reference 19 (Alia et al., 2009).

2.10.2 Cross polarization

In the NMR of solids, cross-polarization (CP) from abundant spins *I* to dilute spins *S* is a double-resonance technique which overcomes two common problems (**Figure 7**).

The first problem is the fact that the solid-state NMR of dilute nuclei such as ^{13}C or ^{29}Si (isotopic abundance of 1.1% and 4.7%) has low sensitivity and these nuclei have a low gyromagnetic ratio. Cross polarization enhances signal from dilute spins potentially by a factor of γ_I / γ_S, where *I* is the abundant spin and *S* is the dilute spin.

Since abundant spins are strongly dipolar coupled, they are therefore subject to rapid spin-lattice relaxation at the abundant nuclei.

Polarization is transferred during the spin locking period, (the contact time) and a $\pi/2$ pulse is only made on protons.

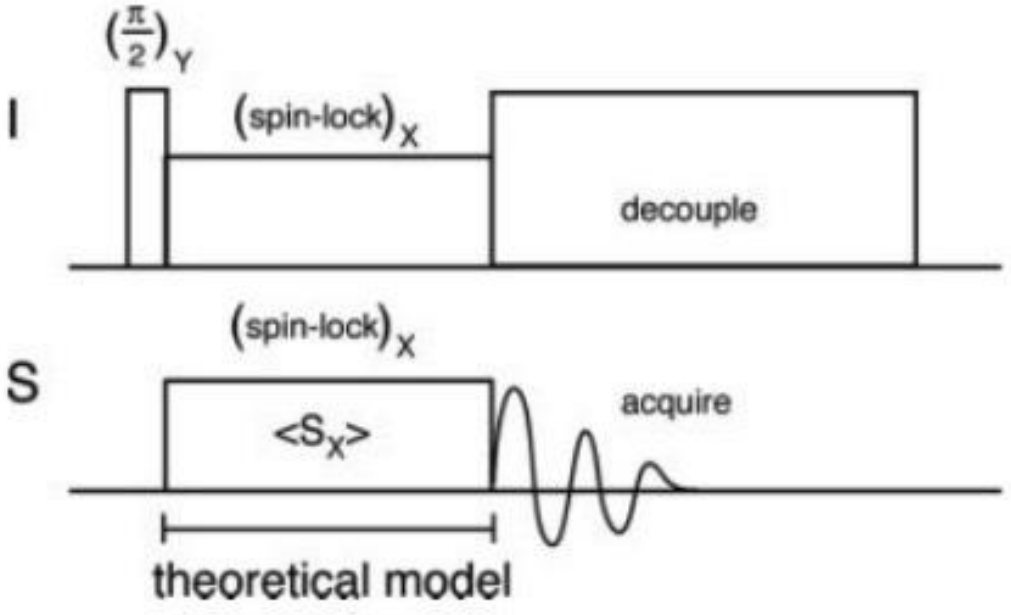

Figure 7. Schematic diagram for experiment employing cross polarization. Reprint from reference 18 (Rovnyak, 2008).

Chapter 3: Introduction to non-covalent interactions and halogen bonds

3.1 Introduction

"*A halogen bond occurs when there is evidence of a net attractive interaction between an electrophilic region associated with a halogen atom in a molecular entity and a nucleophilic region in another, or the same, molecular entity*" (Cavallo et al., 2016).

The halogens (group 17 elements) are diatomic species in their elemental form with the chemical formula X_2 (where X = F, Cl, Br, I). In nature, they are presented as covalent or ionic species and they are found in this manner because of their reactivity. Moving down group 17, the elemental species exist in different phases from gas (F_2 and Cl_2) to liquid (Br_2) to solid (I_2)[7]. Depicted in **Figure 8** are the electrostatic potentials of the trifluoromethane halogens, where the σ-hole is present in red.

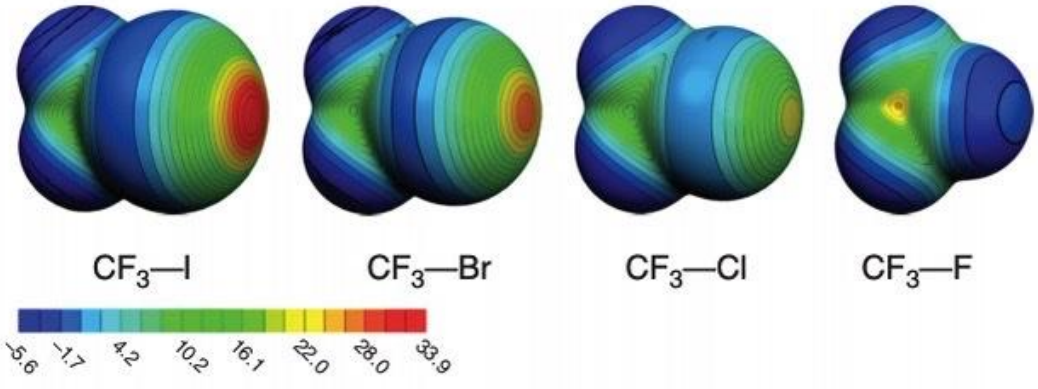

Figure 8. Molecular electrostatic potential maps drawn at the isodensity surface of 0.001 au for CF_3I, CF_3Br, CF_3Cl, and CF_4. All maps are drawn at the same scale, and values are in kcal/mol[7]. Reprinted with permission from reference 7. Copyright 2007 Springer.

3.2 Non-covalent interactions

Non-covalent interactions exist between two different molecules or within a molecule and are the result of the interactions between electrons resulting from their charge distributions over a particular atom or molecule (**Figure 9**).

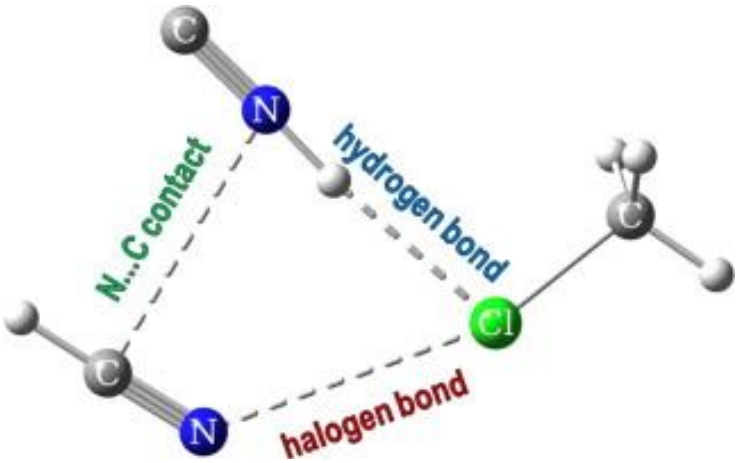

Figure 9. Non-covalent molecular interactions. Reprinted with permission from reference 17 (Domagała et al., 2012).

Supramolecular chemistry and processes are guided by non-covalent interactions, such as van der Waals (vdW) interactions, π-interactions, and electrostatic interactions. Therefore, halogen bonding is an example of a noncovalent interaction; it is where an area of partially positive charge, called a σ-hole, acts as an electrophile for a negatively charged or electron rich molecule.

Electrostatic interactions, such as the dipole-dipole interaction, are examples of an attractive vdW interaction arising due to the electronic dipoles formed from the asymmetric

distribution of electrons over the surface of an atom or a molecule, where some regions tend to be more electronegative than others[20].

Other interactions are very common, the hydrogen bonding exhibit partially non-covalent character, whereby the partially positive charge on the hydrogen atoms can interact with a partially negative charge as shown in **Figure 10** [21].

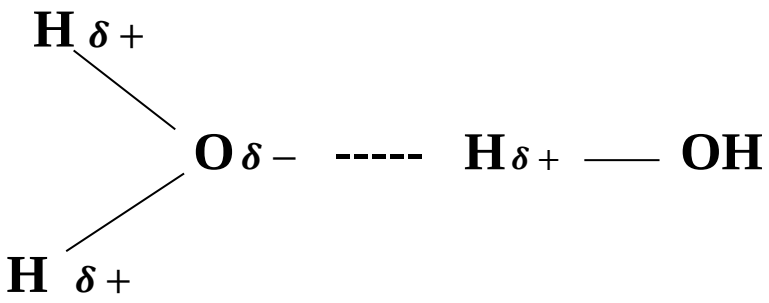

Figure 10. Hydrogen bonds (Steiner, 2002)

The electrostatic interactions between the partially positive (δ^+) and partially negative (δ^-) charge contribute to an attractive interaction between the oxygen and hydrogen atoms in water molecules. The π-interactions may occur between the negative charge distribution on aromatic faces resulting from the π-orbitals, and any partially positive or formally positive counter charge, such as an ion or another aromatic ring. These interactions are quite weak, on the order of 1-3 kcal/mol as shown in **Table 4** [21].

Table 4. Typical interaction strength of noncovalent interactions compared to some examples of covalent bonds. A variety of examples were selected to present an idea of expected interaction energy strengths[22].

Interaction		Interaction Strength/ kcal mol^{-1}
Covalent Bond	C-C	85
	C-H	10
	C=O	175
Hydrogen Bond		1-3
	PH···N	0.8
van der Waals Interactions		0.5-1
Halogen Bond		1-7
	chloro-cyanoacetylene	2.3
Chalcogen Bond	$H_2S\cdots Cl^-$	0.81
	$SCS\cdots Cl^-$	10.59
	$F_4S\cdots NH_3$	14
Pnicogen Bond	FN···N	4
	PN···N	7
	$F_4P\cdots NH_3$	43
	$H_3FP\cdots NH_3$	36

3.2.1 The σ-hole theory

The σ-hole theory explained the behavior of halogen atoms as electrophiles, and it is quite commonly used. The term σ-hole arises due to the region of electron density deficiency occurring along the extension of the R-X σ- bond in the R-X...D model system.

Regularly, covalently bonded halogens are seen as negatively charged entities. However, the polarizability of the halogen atom and its electronegativity are the critical factors in determining the σ-hole's presence or absence and their magnitudes.

When the halogen is more polarizable and has lower electronegativity, the potential of the σ-hole can become more strongly positive, so the positivity of the σ-hole increases in the order F ‹ Cl ‹ Br ‹ I. In other terms, the strength of a σ-hole depends significantly on the electron withdrawing character of its covalently bonded partner atom or molecule.

When a halogen participates in a covalent interaction, an anisotropic charge distribution forms and a positive electrostatic potential appears on the outermost portion of the surface of the σ -hole. The more polarizable the halogen is, the more positive is its σ -hole and stronger is the halogen bond that it forms.

Therefore, the strength of the halogen bond increases in the order of I > Br >> Cl >> F surrendering the lighter halogens to be significantly weaker halogen bond donors. The positive character of the σ -hole can also be increased by making the molecular environment around it more electron withdrawing [23,24].

3.2.2 The halogen bonds

Observations of halogen bonds were first published as early as 1863. It was "rediscovered" because of the interest in crystal engineering, and it has become a topic of growing interest for the past decade[25].

Halogen atoms in haloorganics are considered as sites of high electron density because of their high electronegativity (**Figure 11**). It is commonly accepted that halogen atoms can form attractive interactions by functioning as electron donor sites (i.e., nucleophiles). Nevertheless, the electron density in halogen atoms is anisotropically distributed when the atom is covalently bonded to one or multiple atoms[24].

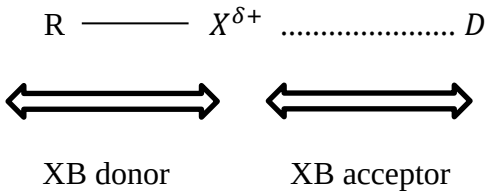

Figure 11. Schematic representation of the R-X-D model used to describe XB.(Clark et al., 2007).

The contacts are electrostatic intermolecular interactions. However, they involve an electron donor and an electron acceptor. The halogen bond donor is an electron acceptor, and the electron donors, act as the halogen bond acceptors, such as nitrogen or oxygen.

There are three types of halogen bonds, the conventional halogen bond, the type-I halogen–halogen, and the type-II halogen–halogen (**Figure 12**).

The conventional halogen-bond is between electronegative atoms such as nitrogen, oxygen or sulfur, and the electron-deficient tip of a halogen atom. The second type is the type-I halogen–halogen contacts due to van der Waals interactions between two halogen atoms. The third type is the type-II halogen–halogen contacts between the electron-rich and electron-deficient regions on a halogen atom. In other terms, the halogen bond is an attractive interaction in which an electrophilic halogen atom approaches a negatively polarized species.

In terms of crystal design, halogen bonds offer a unique opportunity in the strength, atom size and interaction gradation. The halogen bond is a good tool to achieve orthogonality in molecular crystals because of the specific directionality of the halogen bond. Although, by varying these orthogonally oriented halogen···halogen interactions, the mechanical properties can be tuned[7,26,27] .

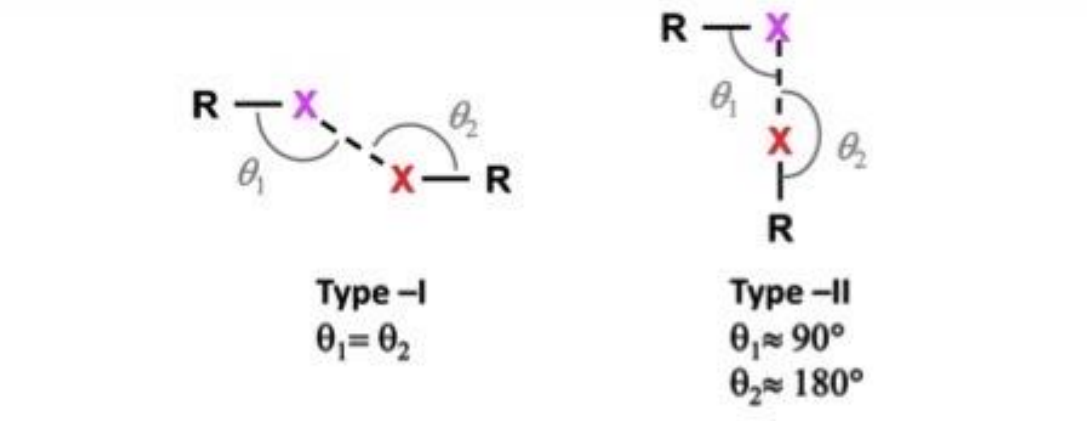

Figure 12. Structural scheme for type I (left) and type II (right) halogen···halogen short contacts. X = halogen atom, and R = C, N, O, halogen atom, etc. Type II contacts are XBs. This figure was taken from : https://pubs.acs.org/doi/10.1021/acs.chemrev.5b00484 and further permission related to the material excerpted should be directed to the ACS.

3.3 Historical Perspective

From two centuries ago, the beginning of the XB story discovered when $I_2 \cdots NH_3$, the first halogen-bonded complex ever prepared, it was synthesized by J. J. Colin while working in the laboratory of J. L. Gay-Lussac[28].

In 1819, P. Pelletier and J. B. Caventou reported the first experimental evidence revealing the ability of dihalogens to interact attractively with anions, they published the synthesis of strychnine triiodide, where the I_3^- anion was formed on interaction of I^- with I_2 [29,30]. In 1870 S. M. Jörgensen proposed that polyiodide alkaloids contain iodide anions as well as I_2 and published the first systematic investigation on the topic[31].

In 1883 O. Rhoussopoulos reported the synthesis of the quinoline/iodoform adduct, showing that halocarbons behave as dihalogens and form adducts with Lewis bases[31]. Then, I. Remsen and J. F. were the first discovered the formation of halogen-bonded complexes involving bromine and chlorine as electron acceptor species at the end of the 19th century by I. Remsen and J. F. Norris has described the 1:1 dimer formed by Br_2 and Cl_2 with various amines[33].

The first XB adduct involving F_2 was reported only 80 years later when it was possible to isolate the F_3^- anion by using very extreme conditions, and the synthesis of $F_2 \cdots NH_3$ and $F_2 \cdots OH_2$ adducts appeared only in the 1990s. The mid-70's, Dumas introduces the term "halogen bonding"[34-37].

In the late 80's, halogen bonding was re-introduced with Desiraju and Legon, and by the late 90's received a lot of interest as Resnati and Metrangolo showed their application in crystal engineering.

Nowadays, it is well established, that the XB strength scales with the polarizability of the XB donor atom, F < Cl < Br < I, so F is the least prone to be involved in XB, being the less polarizable halogen atom, that can act as an XB donor only when attached to particularly strong electron-withdrawing groups[38-41].

3.4. Halogen bond contacts

In the solid-state, halogen bond interactions are symbolized as R-X... Y notation and they are quantified by their contact distance and angle with Lewis base. We can calculate the ratio R_{XA}, that is defined as halogen bond interaction bond:

$$R_{XA} = \frac{d_{XA}}{X_{vdw} + A_{vdw}}$$

where d_{XA} is the measured distance (Å) from the halogen donor (X) to the acceptor (A), divided by the sum of the vdW radii (Å) of X and A ($X_{vdW} + A_{vdW}$), as X is replaced with the atom represents the halogen bond donor, while A represents the atomic symbol of the halogen bond acceptor atom. It is very important to specify the vdW values. Typically, smaller ratio values indicate strong halogen bond interactions[42].

3.5 Halogen bond characteristics

From different studies (Alvarez, 2013; Metrangolo et al., 2008; Priimagi et al., 2013; Riel et al., 2018) , we conclude several features of the halogen bond that should be considered:

a- The halogen bond is highly directional interaction and highly tunable with energies up to 200 kJ/mol.

b- The R-X...Y angle tends to be around 180°.

c- Halogen atoms are more hydrophobic and more polarizable than the hydrogen atoms.

d- Despite the structural differences, both hydrogen and halogen bond donor strength can be tuned in two ways similarly by altering the donors, and by introducing stronger electron-withdrawing groups on the R group.

e- The halogen bond tunability is completed in different ways:

- By changing the halogen, a more polarizable halogen will result in a greater σ-hole.
- By changing the hybridization of the atom bound to the halogen and by changing the atom that the halogen is bound to [43-46].
- The electron-withdrawing is very important factor, by increasing the electron-withdrawing ability of adjacent groups, resulting in a greater σ-hole and to a more powerful interaction. Therefore, an electron-donating species will get the halogen bond weaker[43-46.]

Chapter 4: Cambridge Structural database for polymorphs

4.1 Introduction

After reading the literature, I have found some known halogen bond donors and searched the Cambridge Structural Database (CSD) by drawing the molecules and looked for combinations with halogen bond acceptors to find some polymorphs. I have made a table of 8 pairs and tried to prepare them from according to the literature, by looking for melting points of compounds and checked the conditions of making these polymorphs.

The CSD categorizes structures and polymorphs in different ways. The most familiar to many may be the refcode notation. Although, all structure determinations of a compound are grouped together, including those at different temperatures, pressures, polymorphs etc. In some cases, we rely on the interpretation of the scientists who report the compounds, and later developments may require us to make changes. The CCDC's ConQuest also provides lists to analyze structures and to determine the best example of each unique polymorph. Researchers at the CCDC are also providing tools to help scientists evaluate the stability of their compounds[46]. In the following paragraph, I describe the preparation of polymorphs taken from Table 2 in this work.

4.2 Preparation of known polymorphs

4.2.1 Cocrystal (coumarin)(1,4-diiodotetrafluorobenzene)

a- Method of preparation of pair F (Table 5)

Coumarin (14.6 mg) and 1,4-diiodotetrafluorobenzene (20.1 mg) were dissolved in ethyl acetate (1 mL). The solvent of the solution was allowed to evaporate at room temperature[47].

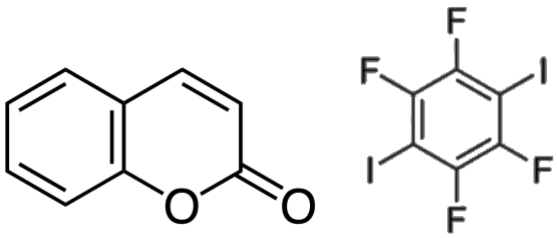

1 **2**

Figure 13. Molecular structures of coumarin (1) and 1,4-diiodotetrafluorobenzene (2).

b- Powder X-ray pattern

The Powder x-ray patterns below in **Figure 14** shows that peaks from the simulated pattern match the ones for the experimental patter. That means the cocrystal structure prepared matches the paper (Cheng et al., 2019).

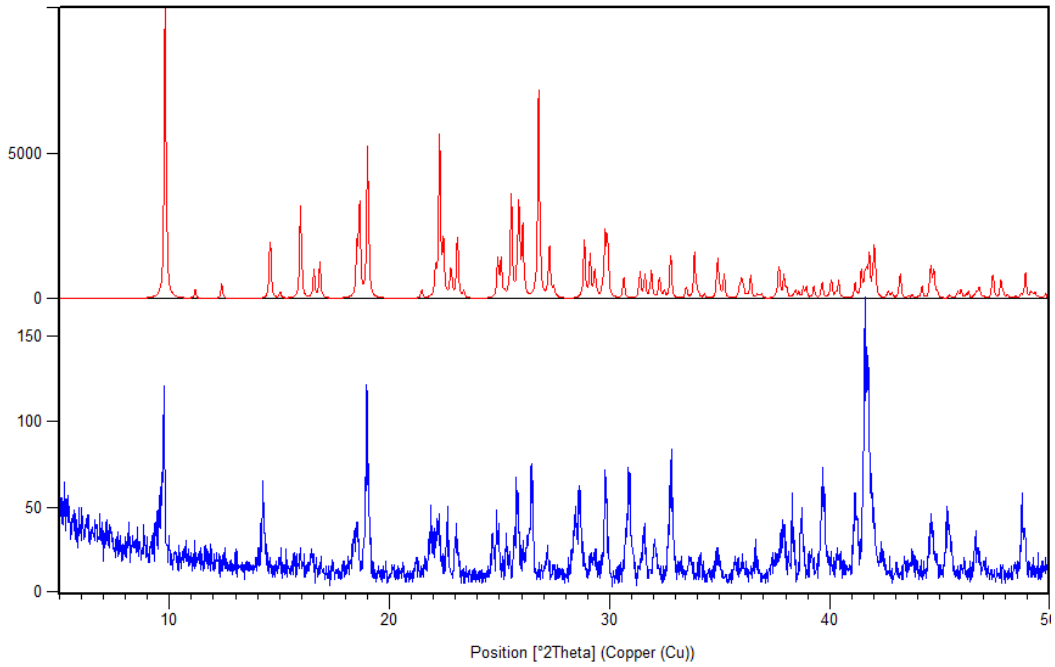

Figure 14. Powder X-ray diffraction patterns. The red one is the simulated pattern, and the blue one is the experimental pattern for cocrystal coumarin and 1,4-diiodotetrafluorobenzene.

c- Purification of compound by vacuum sublimation

I had to purify the compound by vacuum sublimation (**Figure 15**). I placed the sample to be sublimed in the bottom of the sublimation apparatus. After that, I did lightly grease all joints, then I used thick-walled tubing to attach to the vacuum arm and apply the vacuum. Last step was running water through the condenser.

Figure 15. Vacuum sublimation apparatus used.

d- Results

I got a pure cocrystal but little quantity, and unfortunately could not do NMR analysis for the cocrystal. The experimental powder X-ray pattern matched the simulated one, and as result we can say that it is same structure as in the paper (Cheng et al., 2019).

4.2.1 Preparation of other polymorphs

I am showing in this paragraph, a table summarizing the preparation of some polymorphs in **Table 5**, their structures (**Figure 16, Figure 17, Figure 18)** and the results I have gotten.

Table 5. Summary of results for trials in preparing the polymorphs[48,49,]

Polymorphs pairs/ Molecules' Structures	**Methods of preparation and procedures**	**Results**
A-B 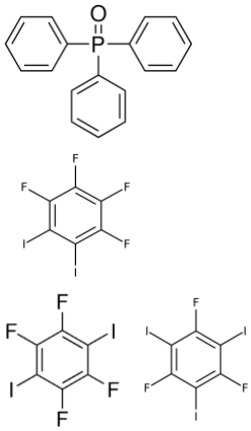	The purchased Ph_3PO, which was a mixture of two polymorphs (monoclinic and orthorhombic), was recrystallized from acetone to give the monoclinic polymorph before use in further reactions. Halogen-bonded compounds were produced by (Liquid assisted grinding) LAG, whereby equimolar amounts of starting material were ground in a mortar and pestle with a trace amount of acetonitrile for about 20 min.	I obtained the Ph_3PO experimental powder X-ray pattern and matched the simulated one, but I did not obtain the crystal structures for the polymorphs A and B.
E-F 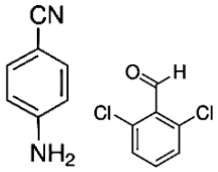	The 2,6-dichlorobenzaldehyde (0.36 g) was added to the ethanolic solution (20 ml) of 4-amino-benzonitrile (0.24 g) with few drops (1 ml) of glacial acetic acid. The mixture was stirred for 5h at 80°C under reflux (**Figure 20**) and then was cooled by putting it in freezer/fridge for one week (Different trials shown in **Table 6,** then it was filtered, washed with ethanol and water (1/1) and dried in vacuum. The filtrate was left over to room temperature 7 days.	I got a powder not a crystal, I did analyze the product but unfortunately based on Powder X-ray results did not get what is expected the structure obtained in paper did not match the one I obtained. PXRD results shown in **Figure 21.**
G- H 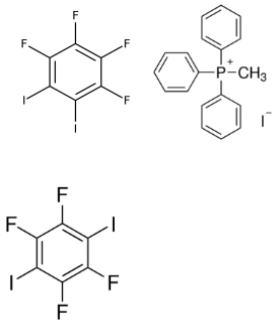	-Preparation of PPh_3MeI_3. (*p*-F_4 DIB): (Ph3Me) P^+I^-(10.00 mg, 0.025 mmol) was dissolved in ethanol (4 ml, 98%) and I_2 (6.27 mg, 0.025 mmol) was added to that solution followed by addition of DCM (4 ml). Then *p*-F_4DIB (9.941 mg, 0.025 mmol) and acetonitrile (4 ml) were added to the solution after stirring	I got a powder, it looked like precipitation I have noticed that maybe something related to starting material I used, maybe the starting materials are not pure, I had run the PXRD for it and it is shown in **Figure 22**.

	the solution. Allow the solution to evaporate. - Preparation of Ph_3MeI_3. (*o*-F_4DIB) and PPh_3MeI_3. 2(*o*-F_4DIB): (Ph_3Me) P+I^-(10.00 mg, 0.025 mmol) was dissolved in ethanol (4 ml, 98%) and I_2 (6.27 mg, 0.025 mmol) was added to that solution followed by addition of DCM (4 ml). Then *p*-F_4DIB (19.88 mg, 0.05 mmol) and acetonitrile (4 ml) were added to the solution after stirring the solution. Allow the solution to evaporate. - Preparation of 2(C_{19} H_{18} P) $^+$ 2 (I_3)$^-$. 3(C_6 F_4 I_2): (Ph3Me)P^+I^- (10.00 mg, 0.025 mmol) was dissolved in ethanol (4 ml, 98%) and I_2 (6.27 mg, 0.025 mmol) was added to that solution followed by addition of DCM (4 ml). Then *σ*-F_4DIB (19.88 mg, 0.05 mmol) and acetonitrile (4 ml) were added to the solution after stirring the solution. Allow the solution to evaporate.	

Table 6. Different trials for preparation of polymorphs E-F (Benarous et al., 2016).

Trial 1	Trial 2	Trial 3	Trial 4
5 drops of glacial acetic acid	1 drop of glacial acetic acid	1 drop of glacial acetic acid	1 drop of glacial acetic acid
stirred for 3h at 90° C	stirred for 3 h at 100° C (Rotovap)	stirred for 3 h at 78° C	stirred for 3 h at 100° C under argon

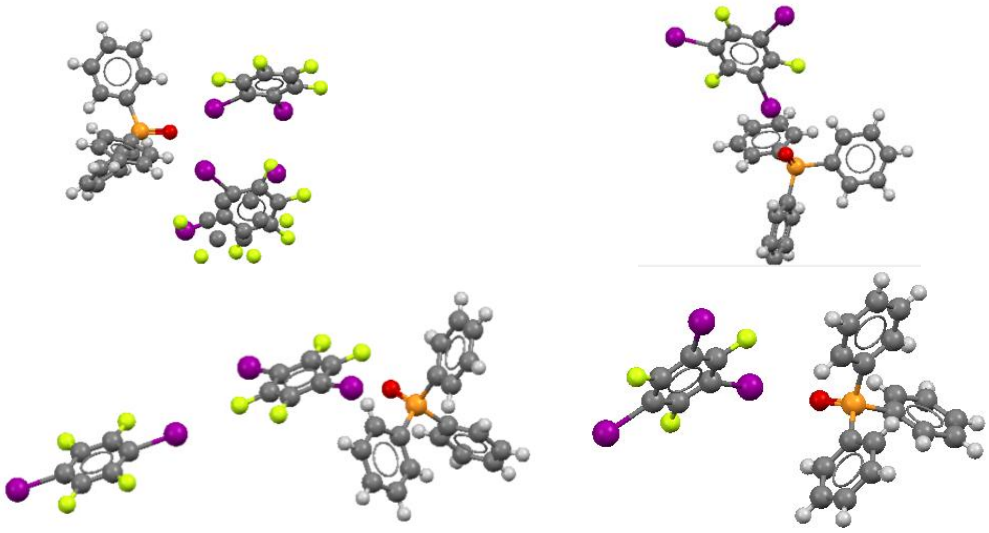

Figure 16. The molecular structures for pairs of polymorphs A and B: 1) and 2) $C_{18}H_{15}OP$, 2($C_6F_4I_2$)- 3) and 4) $C_{18}H_{15}OP$, $C_6F_3I_3$.(Kobra et al., 2018; Xu et al., 2015).

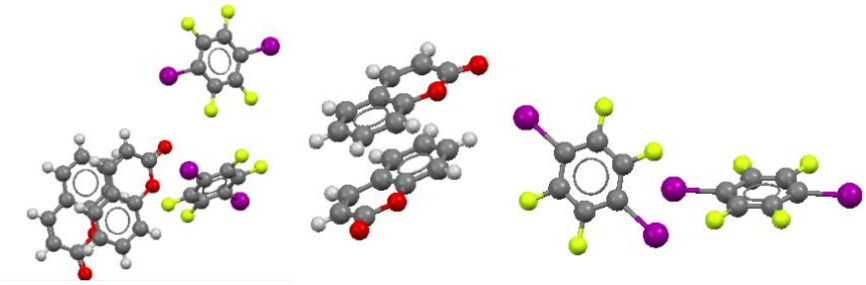

11 **12**

Figure 17. The molecular structures for pairs of polymorphs E, F: 11) and 12) 2($C_9H_6O_2$), $C_6F_4I_2$(Benarous et al., 2016).

13 **14** **15**

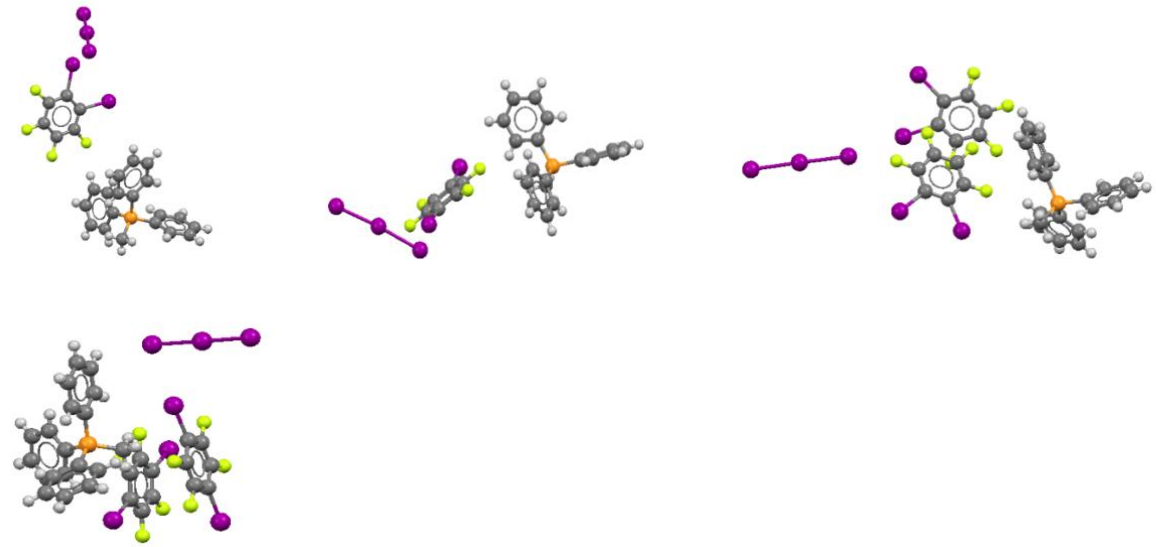

16

Figure 18. The molecular structures pair of polymorphs G and H: 13) and 14) $(C_{19}H_{18}P)^+I_3^-$. ($C_6F_4I_2$)- 15) $C_{19}H_{18}P)^+(I_3)^-$.2($C_6F_4I_2$) and 16) 2$(C_{19}H_{18}P)^+$2 $(I_3)^-$.3($C_6F_4I_2$)(Kobra et al., 2018).

Figure 19. Experimental technique used to get the polymorph pairs E and F; the powder obtained - photos taken during the work in laboratory(Benarous et al., 2016).

Figure 20. Synthesis of (E)-2-((2, 6-dichlorobenzylidene) amino) benzonitrile, under reflux for more than 5 hours.

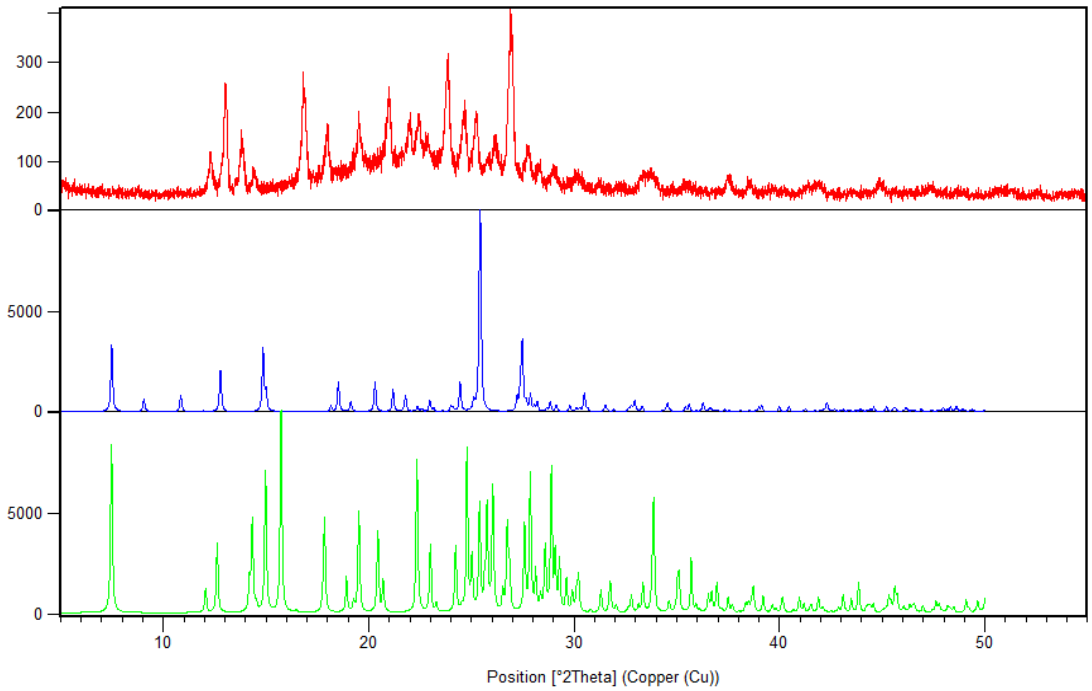

Figure 21. Powder X-ray diffraction patterns. The red one is the experimental pattern of compound obtained, the blue/green are the simulated patterns for polymorphs **E** and **F**, respectively (Benarous et al., 2016).

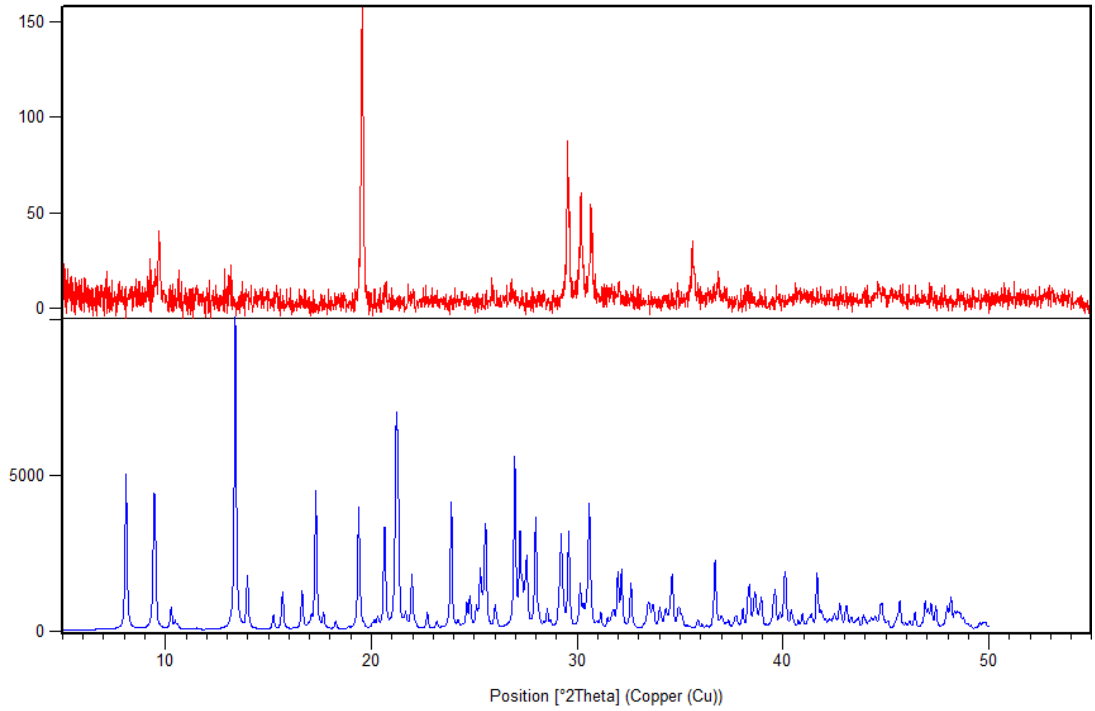

Figure 22. Powder X-ray diffraction patterns, the red one is the experimental pattern, the blue one is the simulated pattern for polymorphs **G** or **H**(Kobra et al., 2018).

4.3 Conclusion

In this chapter, I showed all trials, the successful ones, and non-successful ones. I have tried to reproduce these polymorphs listed in table 5. These are the reasons why not all the polymorphs in my list were obtained:

1- The amounts of compounds obtained should be sufficient to be able to characterize them by Powder X-ray and Solid-State NMR.

2- Some starting materials were not pure, and the compounds I obtained were melted and not co-crystallized.

3- Some other factors also could affect my results, the rate of evaporation that can be affected by changes of temperature and humidity in the room.

4- Some details were missing in papers as the duration of reflux per example.

Finally, we can say by trying those techniques to prepare some polymorphs, I have practiced some cocrystallization methods (vacuum sublimation and slow evaporation) , some purification methods and Rota-evaporation.

Chapter 5 : Experimental results

5.1. Introduction

In previous chapters, I have explained some theories on halogen bonding and polymorphism, the method of preparation of polymorphs, and the characterization methods. In this chapter, I am elaborating the experimental part of my work. The results and analysis of these results are illustrated with some figures of cocrystals, PXRD patterns, and NMR spectra. I discovered new polymorphs in halogen bonded cocrystals, but some trials were unsuccessful, due to different factors as changes in room humidity and in room temperature, the rate of evaporation, type of solvent used, all these factors affect the stability of cocrystals. Please note that I am showing in this chapter some figures taken from my own publications. (Hajjar et al., n.d.) (Hajjar et al., 2021).

5.2 Materials and chemicals used

1,4-diiodotetrafluorobenzene (**1**), 3-nitropyridine **(2)** and coumarin **(5)** were purchased from Sigma-Aldrich. 1,3,5-trifluoro-2,4,6-triiodobenzene **(3)** and piperazine **(4)** were purchased from Alfa Aesar. All compounds were used without further purification.

5.3 Experimental procedures

5.3.1 Sample preparation

In a typical procedure, cocrystal **A** was obtained from the slow evaporation of a solution of the donor **1** (0.1060g mg, 0.3 mmol) and 3-nitropyridine **2** (0.1096 mg, 0.3 mmol) in ethanol at room temperature.

Cocrystal **B** was obtained from the slow evaporation of a solution of the donor **3** (0.025 g in 1 mL chloroform) and a molar excess of halogen bond acceptor **4** (0.0412 g in 1 mL ethanol) at room temperature. The two solutions were prepared independently and stirred. After dissolution, the two solutions were mixed, stirred, and covered to allow for slow evaporation and crystal formation. Cocrystal **C** was obtained from the slow evaporation of a solution of the donor **1** and 3-nitropyridine **2** in dichloromethane (1 mL) at room temperature in a 2:1 molar ratio. Cocrystal **D** was obtained from the slow evaporation of a solution of the donor **1** and 3-nitropyridine **2** in a 1:1 molar ratio in ethanol (1 mL) at room temperature.

Cocrystal **E** was obtained from the slow evaporation of a solution of donor **1** (20.1 mg) and coumarin **5** (14.6 mg) were dissolved in ethyl acetate (1 mL). at room temperature in a 2:1 ratio and the nomenclature of my compounds was taken from **Table 1**.

5.3.2 Other trials and techniques for preparation of cocrystals

In laboratory, I have tried different methods of preparation of cocrystals. **Table 7** summarizes these methods, which compounds I have used, and the amounts of starting materials used. Although, I am explaining in the next paragraph the ball milling method, and co-sublimation method. The slow evaporation method, vacuum sublimation, cooling and vapor diffusion methods are explained in chapter 2. In **Figure 23** cocrystals prepared by cooling method are shown.

Table 7. Amounts of Starting Materials for cocrystals synthesis.

Techniques	Halogen Bond donors (g)	Halogen Bond acceptors (g)	Conditions/ solvents	Results
Mechanochemistry method (Ball milling)	1,3,5-trifluoro-2,4,6-triodobenzene 0.1941 g	Piperazine 0.105 g	Frequency 25 Hz for 30 minutes	unsuccessful
	1,3,5-trifluoro-2,4,6-triodobenzene 0.242 g	Piperazine 0.017 g	Frequency 20 Hz for 25 minutes	unsuccessful
Cosublimation	1,3,5-trifluoro-2,4,6-triodobenzene 0.036g	Piperazine 0.039g		unsuccessful
Slow evaporation	1,3,5-trifluoro-2,4,6-triodobenzene 0.02518g	Piperazine 0.0412 g	Chloroform/ Ethanol	**successful**
	1,3,5-trifluoro-2,4,6-triodobenzene 0.2 g	Piperazine 0.04 g	Acetonitrile	unsuccessful

Vacuum Sublimation	1,3,5-trifluoro-2,4,6-triodobenzene 0.1942g	Piperazine 0.1082g		unsuccessful
Slow evaporation	1,4-diiodotetrafluorobenzene 0.11g	3-nitropyridine 0.11g	Ethanol	**successful**
	1,4-diiodotetrafluorobenzene 0.1g	3-nitropyridine 0.1g	Ethanol	**successful**
	1,4-diiodotetrafluorobenzene 0.29g	3-nitropyridine 0.04g	dichloromethane	**successful**
	1,4-diiodotetrafluorobenzene 0.2506g	3-nitropyridine 0.078g	Ether	unsuccessful
Cooling	1,4-diiodotetrafluorobenzene 0.11 g	3-nitropyridine 0.13 g	Ethanol fridge	unsuccessful
Mechanochemistry method (Ball milling)	1,4-diiodotetrafluorobenzene 0.266g	3-nitropyridine 0.0475g	Frequency 25 Hz for 25minutes	unsuccessful

Vapor diffusion	1,4-diiodotetraflu-robenzene 0.25g	Piperazine 0.01g	Hexane/chloroform	unsuccessful
Liquid assisted grinding (LAG)	1,4-diiodotetraflu-orobenzene 0.2506 g	3-nitrpyridine 0.078 g	Frequency 25 Hz for 25minutes +20 microliters ethanol	unsuccessful
Liquid Assisted grinding (LAG)	1,4-diiodotetraflu-orobenzene 0.266 g	3-nitrpyridine 0.475 g	Frequency 25 Hz for 25 minutes +20 microliters ethanol	unsuccessful

Figure 23. Different crystals photos prepared by cooling method.

5.3.3 Ball milling method

The mechanochemical preparation of some cocrystals mentioned in **Table 7** was performed using a Retsch MM400 ball mill as shown in **Figure 24**. Both the halogen bond donor and the appropriate halogen bond acceptor were added as powders successively to a stainless-steel milling jar in their proper stoichiometric ratio. All experimental masses can be found in **Table 7**. Ball milling was performed with a milling frequency of 25 Hz for a 30-minute period and some cocrystals were performed for 25 minutes at room temperature using two stainless steel grinding balls[10].

Figure 24. Photo taken of Retsch MM400 ball mill.

5.3.4 Cosublimation method

The halogen bond donor and acceptor were added separately to the ends of a 2.5 mm diameter glass tube (**Figure 25**). This latter was then sealed in vacuo. In a two-zone tube furnace, the temperature of each end of the tube was monitored separately, where the zone containing starting material 1 was heated from room temperature to an initial temperature

of 20 °C below the melting point and slowly raised to a temperature of 20 °C above the melting point at a rate of 0.05 °C/min. Each end of the sublimation tube was held at final temperatures for 10 h and was allowed to slowly return to room temperature for 7 to 10 hrs. Then, the cocrystal was collected near the center of the tube[50].

a

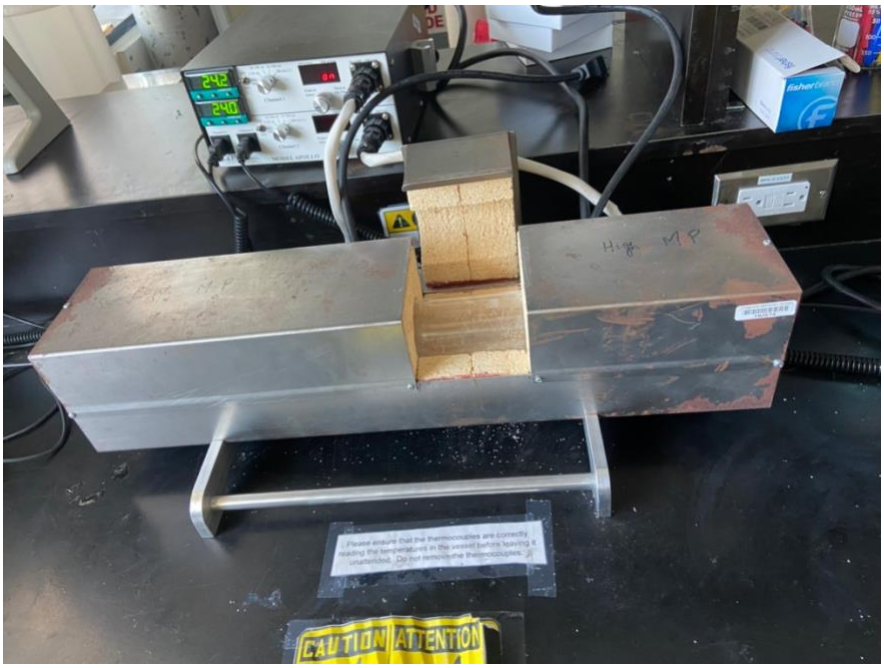

b

Figure 25. (a) Cosublimation apparatus (b) Empty 25 cm thin-necked glass tube. The halogen-bond donor and acceptor are added to opposite extremities of the tube and sealed in vacuo.

5.4. Solid-State Nuclear Magnetic Resonance Spectroscopy

$^{1}H \rightarrow ^{13}C$ CP/MAS SSNMR experiments were performed at 9.4 T on a Bruker Avance III spectrometer, using a Bruker 4 mm HXY MAS probe with a spinning frequency of 10 to 12 KHz. Chemical shifts were referenced to glycine at 176.4 ppm relative to tetramethylsilane (TMS). The $^{19}F \rightarrow ^{13}C$ CP/MAS SSNMR experiments were performed at 11.7 T on a Bruker Avance spectrometer, using a Bruker 4 mm HXY MAS probe with various spinning speeds. The spectra were referenced to powdered polytetrafluoroethylene at 111.3 ppm relative to TMS. In **Table 8** , we summarize the NMR data for cocrystals B, C, D (recycle delay, contact time, number of scans, 90-degree pulse, pulse program, acquisition time, spinning speed and decoupler pulse length.

Table 8. Solid-State nuclear magnetic resonance spectroscopy experiment information.

Compounds	Recycle delay	90-degree pulse	Contact time	Pulse program	Decoupler pulse length	Acquisition time	Number of scans	Spinning speed
3-nitropyridine	10	3.5	5	CP/MAS (^{1}H to ^{13}C)	7	50	9974	10
	2	3.5	8	CP/MAS (^{1}H to ^{13}C)	7	50	44374	9
1,4-diiodotetrafluo-robenzene	180	3.5	5	CP/MAS (^{19}F to ^{13}C)	6.75	40	31	10
	10	1.79	-	Zg (^{19}F)	-	20	16	10
Polymorph B	2	3.9	2	CP/MAS (^{1}H to ^{13}C)	7	50	38912	9

	60	3.45	5	CP/MAS (^{19}F to ^{13}C)	6.75	40	2048	10
	100	3.45	4	Zg (^{19}F)	8	20	2	10
Polymorph C	120	3.5	4	CP/MAS (^{1}H to ^{13}C)	7.5	40	743	11
	15	3.5	7.5	CP/MAS (^{1}H to ^{13}C)	7	50	5100	9
	60	3.45	5	CP/MAS (^{19}F to ^{13}C)	6.75	40	1496	10
	180	3.5	5	CP/MAS (^{19}F to ^{13}C)	6.75	40	500	12
	100	3.45	-	Zg (^{19}F)	-	20	2	10
Polymorph D	30	4.02	3	CP/MAS (^{1}H to ^{13}C)	7.05	50	4096	7
	60	4.02	3.5	CP/MAS (^{1}H to ^{13}C)	7.05	50	3057	9
	180	3.5	5	CP/MAS (^{19}F to ^{13}C)	6.75	40	367	12
	100	3.45	5	CP/MAS (^{19}F to ^{13}C)	6.75	40	819	10
	5	3.45	-	Zg (^{19}F)	-	20	2	10

5.4 Discussion and Analysis of results

Cocrystal **A** has a stoichiometry of two molecules of 3-nitropyridine to one molecule of 1,4-diiodotetrafluorobenzene and was obtained via slow evaporation from ethanol. SCXRD shows that this stoichiomorph packs in the monoclinic *Cc* space group with a large unit cell of 9896.3(14) Å (**Figure 26**)

There are ten crystallographically distinct C-I...N halogen bonds between 1,4-diiodotetrafluorobenzene and 3-nitropyridine molecules as summarized in **Table 11**. Each iodine atom of the halogen bond donor interacts with a ring pyridyl atom. Interestingly, none of the atoms of the nitro group engage in halogen bonding. The halogen bonds in cocrystal **A** range in distance from 2.865 to 2.990 Å and the C-I···N angles range from 169.6 to 174.9°. These distances represent a range of reduced distance parameters, R_{XB}, ranging from 0.81 to 0.85.

Table 9. Selected X-ray Crystallographic Data for the cocrystals Studied Herein (Hajjar et al., n.d., 2021) (Hajjar et al., 2021).

	A	B	C	D
Formula	C_6 F_4 I_2, 2(C_5 H_4 N_2 O_2)	C_4 H_{10} N_2,2(C_6 F_3 I_3)	2(C_6 F_4 I_2), (C_5 H_4 N_2 O_2)	C_6 F_4 I_2,2(C_5 H_4 N_2 O_2)
Space Group	Cc	P-1	P-1	P21/n
Cell lengths	a 6.1328(5) b 54.226(4) c 29.852 (2)	α 8.6450(5) β 9.1660(5) c 9.3403(5)	a 7.5779(9) b 7.8895(10) c 13.6245(17)	a 10.889(5) b 5.277(2) c 16.830(8)
Cell Angles	α 90 β 94.548(5) γ 90	α 67.4330(10) β 72.8870(10) γ 63.0620(10)	α 76.189(3) β 80.848(3) γ 63.945(3)	α 90 β 94.294(5) γ 90
Cell Volume	9896.24	602.747	709.242	964.358
Z, Z’	Z: 20 Z': 0	Z: 1 Z’:0.5	Z: 2 Z': 0	Z: 2 Z’: 0.5
R-factor	6.29	2.5	2.43	4.3
CCDC identifier	2101747	2101749	2101748	2101750

The value of R_{XB} is calculated as the ratio of the halogen bond distance to the sum of the van der Waals radii of the interacting atoms. Additional weak non-covalent interactions are also noted between pyridyl ring hydrogen atoms and nearby fluorine atoms of **1** (~2.5 Å), as well as between pyridyl ring hydrogen atoms and one of the nitro oxygen atoms (~2.5 to 2.6 Å).

Despite repeated attempts, it was not possible to produce enough cocrystal **A** in powdered form for either PXRD or solid-state NMR characterization.

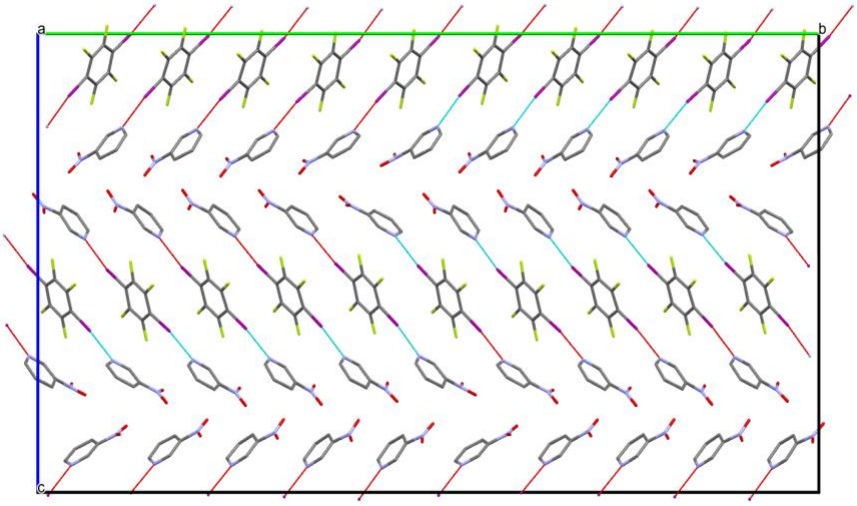

Figure 26. Unit cell of polymorph **A** (S0570) as seen along the axis. Halogen bonds are indicated by dashed red and turquoise lines.

Cocrystal **D** has a stoichiometry of one molecule of 3-nitropyridine to one molecule of 1,4-diiodotetrafluorobenzene, also it has obtained via slow evaporation from ethanol. SCXRD shows that this stoichiomorph packs in the monoclinic $P2_1/n$ space group.

There is a single crystallographically distinct C-I···N halogen bond between 1,4-diiodotetrafluorobenzene and 3-nitropyridine characterized by 2.896 Å (R_{XB} = 0.82) and an angle of 175.6° (**Table 11, Figure 27**). Neither of the nitro oxygen atoms forms a halogen bond to iodine. Instead, some short intermolecular oxygen-hydrogen contacts are noted (~2.6 Å).

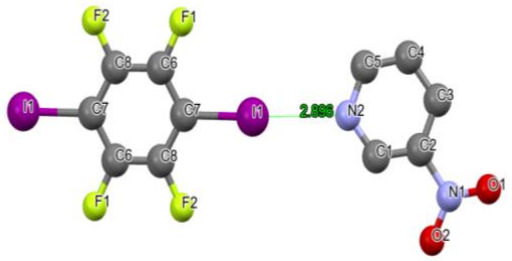

Figure 27. Halogen-bonded network of polymorph **D** (S0872). The I1-N2 distance is shown.

Cocrystal **C** was obtained via slow evaporation from dichloromethane and has a stoichiometry of two 1,4-diiodotetrafluorobenzene molecules to one molecule of 3-nitropyridine. SCXRD shows that this system packs in the triclinic *P* space group. There is a single crystallographically distinct C-I···N halogen bond between 1,4-diiodotetrafluorobenzene and 3-nitropyridine characterized by 2.940 Å (R_{XB} = 0.83) and an angle of 175.4° (**Table 11**; **Figure 28**).

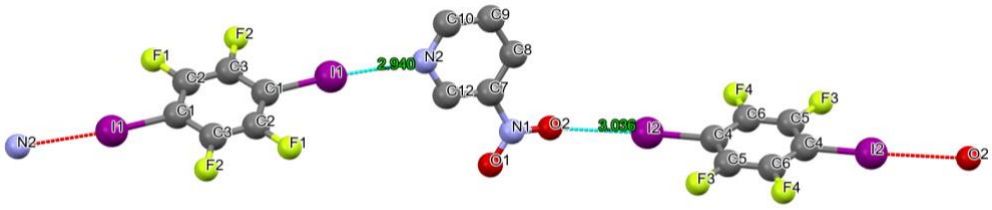

Figure 28. Halogen-bonded network of polymorph **C** (S0790). The I1-N2 distance and I2-O2 distances are shown.

In addition, this stoichiometric cocrystal is the only one of the three studied in this work to feature a halogen bond between iodine and one of the oxygen atoms of the nitro group. The two distinct halogen bonds result in the formation of chains of molecules. The C-I···O halogen bond is characterized by 3.036 Å (R_{XB} = 0.867) and an angle of 177.5°. **Figure 29** shows the photos of cocrystals A, B, C, D obtained and the experimental procedures of making these cocrystals are mentioned in paragraph 5.3.

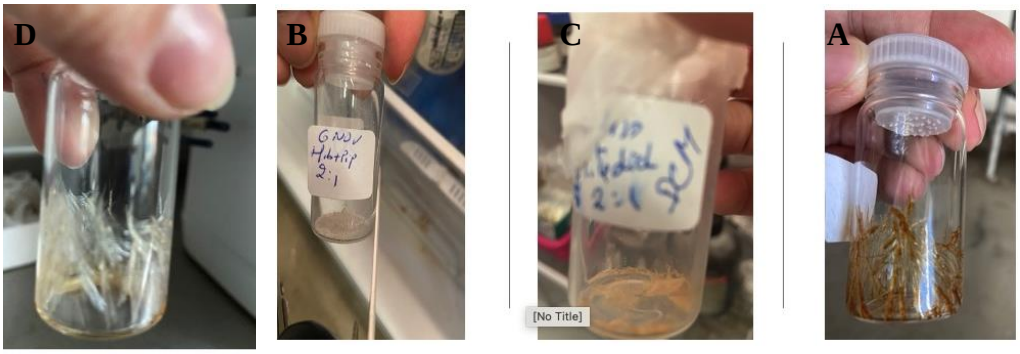

Figure 29. Some photos of cocrystals (A, B, C, D).

Cocrystal **B**, which has a 2:1 1,3,5-trifluoro-2,4,6-triiodobenzene:piperazine (1,4-diazacyclohexane) stoichiometry, features a halogen bond between I1 as the halogen-bond donor and N1 as the halogen-bond acceptor. The iodine–nitrogen distance is 2.820 (3) Å, which corresponds to 80% of the sum of their van der Waals radii.

This is somewhat shorter than the analogous iodine–nitrogen halogen bonds in cocrystals formed from the same halogen-bond donor with acridine (3.022 Å), 1,10-phenanthroline (3.020 and 3.148 Å), or 2,3,5,6-tetramethylpyrazine (2.991 and 2.993 Å), but comparable to those formed with hexamethylenetetramine (2.864 and 2.879 Å) as the electron donor [8].

Comparable distances are also noted in an interesting class of halogen-bonded tubular structures formed from the self-assembly of 1,4-diiodo-tetrafluorobenzene and piperazine cyclophanes. The C1—I1···N1 halogen bond angle in **B** is 178.0 (1) °, consistent with the linear interaction of nitrogen via a σ-hole opposite the carbon–iodine covalent bond. I1 also shows a short contact with C7 of the piperazine molecule of 3.578 (4) Å (**Table 11**); this represents approximately 97% of the sum of their van der Waals radii and is likely a structural consequence of the formation of the adjacent halogen bond rather than a structure-directing element in and of itself.

Possible weak hydrogen bonds are also observed between H1 and I2, between H7A and F2, between H7AB and I3, between H8A and I2, and between H8AB and I1 (**Table 12**). Interestingly, no halogen bonds involving I2 and I3 are observed, even though they are chemically identical to I1.

The structure packs in the triclinic $P\bar{1}$ space group and the aromatic molecules lie in layers (

Figure 30). The stoichiometry of the cocrystal is highlighted by noting that pairs of aromatic molecules lying in adjacent layers are connected to each other via halogen bonding to a single common piperazine molecule.

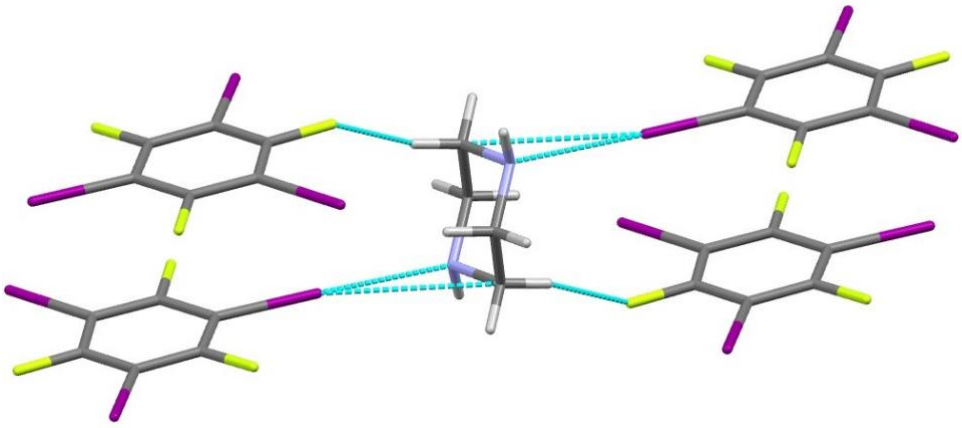

Figure 30. Detail of the X-ray crystal structure for cocrystal **B**, depicting a halogen bond between iodine and nitrogen, a short contact between iodine and carbon, and a short contact between hydrogen and fluorine. The other two iodine atoms on the aromatic ring to not engage in any halogen bonding or other close contacts (Hajjar et al., 2021)

5.5 Powder x-ray diffraction

Crystals were gently ground into fine powders with a mortar and pestle for powder XRD and SSNMR experiments. The crystal structure for each powdered sample was verified by powder X-ray diffraction on a Rigaku Ultima IV instrument with 2 ranging from 5 to 55º in increments of 0.02º using $Cu\ K^{\alpha}$ radiation to ensure phase purity.

Cocrystal **C** was prepared in powdered form as well, and PXRD shows a good agreement between the diffractogram predicted from the SCXRD structure and that obtained experimentally, despite poor signal-to-noise **(Figure 31**). These data confirm that

the polymorphic form of the crystal was retained upon light grinding with a mortar and pestle.

We have noticed after analyzing the data, that cocrystal **D** was reproducibly prepared in quantities sufficient for characterization by PXRD.

As seen in **Figure 32**, the polymorph which was characterized via SCXRD is also obtained in powder form; manual grinding with a mortar and pestle for PXRD experiments did not alter the polymorphic form.

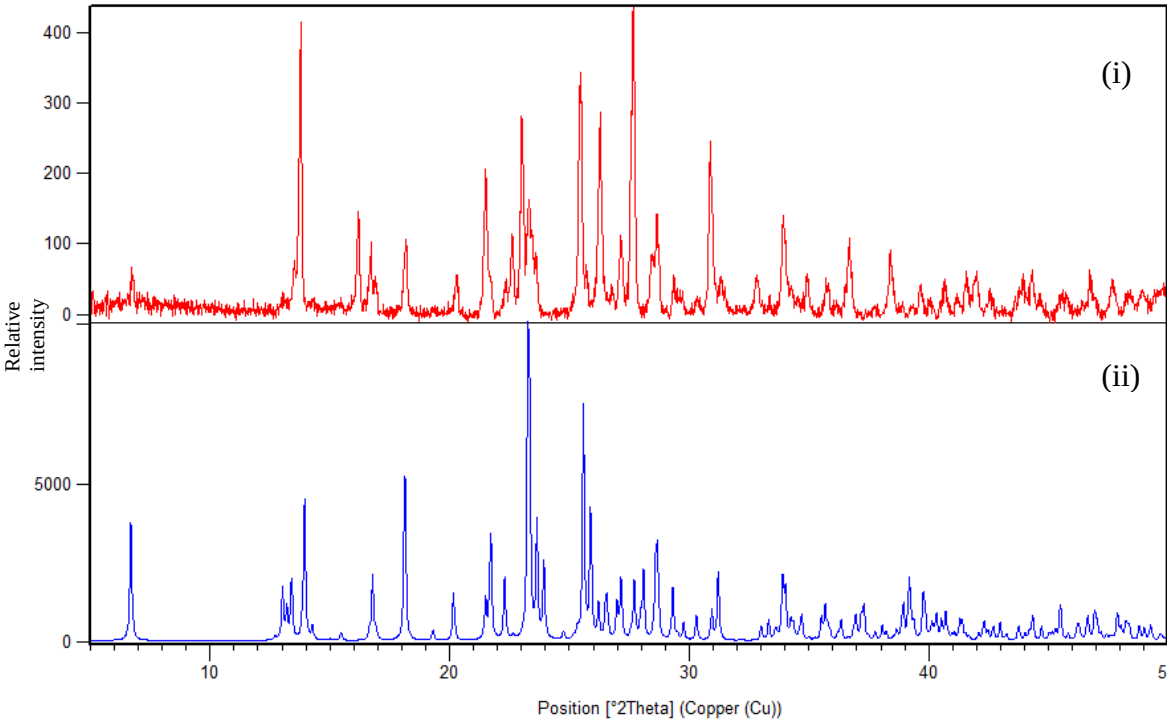

Figure 31. Experimental (i) and simulated (ii) powder X-ray diffraction patterns for cocrystalline stoichiomorph **C**.

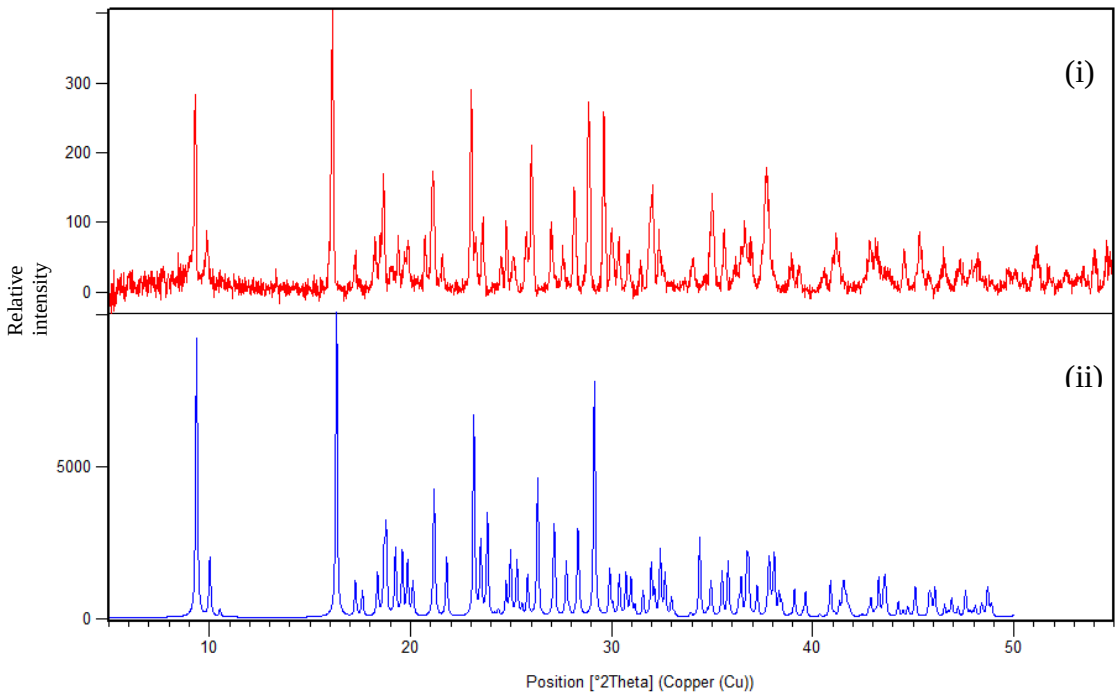

Figure 32. Experimental (i) and simulated (ii) powder X-ray diffraction patterns for cocrystalline stoichiomorph **D**.

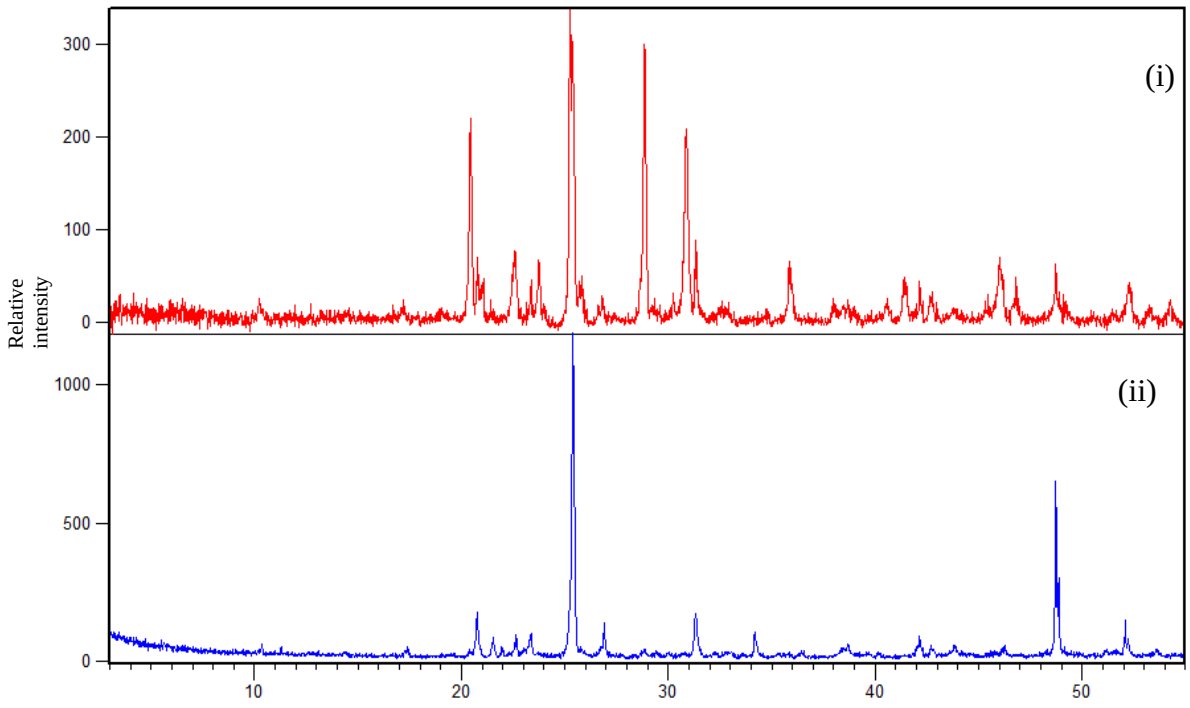

Figure 33. Simulated (i) and experimental (ii) powder X-ray diffraction patterns for cocrystal **B**.

5.6 Single -Crystal X-ray diffraction

Data were collected on a Bruker SMART APEXII single-crystal diffractometer equipped with a sealed tube Mo Kα source (λ= 0.71073 Å), a graphite monochromator, and an APEXII CCD detector. Samples were held at low temperature using a dry compressed air-cooling system. Raw data collection and processing were performed with the *APEX3* software package from Bruker [53].

Initial unit-cell parameters were determined from 36 data frames from select ω scans. Semi-empirical absorption corrections based on equivalent reflections were applied[54]. Systematic absences in the diffraction dataset and unit-cell parameters were consistent with the assigned space group. The initial structural solutions were determined using *SHELXT* direct methods[55]and refined with full-matrix least-squares procedures based on F_2 using *SHELXL* and *ShelXle*[56].Hydrogen atoms were placed geometrically and refined using a riding model. For cocrystal **B**, crystallographic data were collected from single crystals mounted on MiTeGen MicroMounts using parabar oil. Cocrystal A was refined as an inversion twin. Hydrogen atoms were placed geometrically and refined using a riding model.

5.7 Solid-State Nuclear Magnetic Resonance Spectroscopy

The $^{19}F\rightarrow{}^{13}C$ CP/MAS and $^{1}H\rightarrow{}^{13}C$ CP/MAS NMR spectra of a powdered sample of cocrystal **D** are presented in **Figure 34 (b, c).**

The $^{19}F\rightarrow{}^{13}C$ CP/MAS NMR spectrum of pure 1,4-diiodotetrafluorobenzene is also presented in **Figure 34 (a)** for comparison purposes. **In Figure 34 (b)**, the $^{19}F\rightarrow{}^{13}C$ CP/MAS experiment cleanly selects for those carbon atoms which are on the diiodotetrafluorobenzene ring and suppresses those which are on the 3-nitropyridine molecule.

This is attributed to the mechanism of polarization transfer from ^{19}F to ^{13}C, namely via the through-space dipolar interaction which is apparently too weak in this case to polarize ^{13}C spins on the spatially distant 3-nitropyridine molecule. This has been used

previously as a spectral editing tool in various halogen-bonded cocrystals and is again shown to be useful in the present case.

In addition to the dominant aromatic C-F resonances at ~147 ppm, a weaker and broader peak at ~77 ppm is attributed to the carbons directly bonded to iodine (see **Table 10**). This substantial frequency shift is due to relativistic heavy-atom effects on light-atom shielding (HALA) effects [57,58,59,60]of the heavy ^{127}I nuclide on ^{13}C and has been noted previously in several halogen-bonded systems[8,10,52,61]. A close inspection of the C-I peaks for pure 1,4-diiodotetrafluorobenzene and that for cocrystal **D** reveals only a very small change in peak position, from 76.8 ± 1.4 ppm to 77.2 ± 1.5 ppm. The shift to higher ^{13}C frequencies upon formation of a halogen bond to iodine is consistent with several previous reports.

It should be noted that a previous multifield study of the ^{13}C resonance in 1,4-diiodotetrafluorobenzene enabled a proper measurement of the actual isotropic chemical shift rather than simply the peak position; these may not necessarily coincide (and are likely to have different errors) due to residual dipolar coupling to ^{127}I, which is a spin-5/2 nucleus with 100% natural abundance.

Thus, while the errors assigned to these peak positions are large to reflect the fact that the peak positions are not necessarily the exact chemical shift values, a small shift of the peak maximum from 76.8 to 77.2 ppm is clearly observed presently.

The ^{1}H→ ^{13}C CP/MAS NMR spectra of cocrystal **D** (**Figure 34**, **c**) also show that this method is a useful spectral editing tool in cocrystals, selecting only for the 3-nitropyridine molecules. The fact that this spectrum was obtained at room temperature with MAS is further proof of cocrystal formation, as the acquisition of ^{1}H→ ^{13}C CP/MAS NMR spectra

of pure 3-nitropyridine would require cooling due to a melting point for the latter of 35 to 40°C.

^{13}C NMR line widths of approximately 125 to 180 Hz are also consistent with the formation of a solid cocrystal incorporating 3-nitropyridine; line widths for melted pure 3-nitropyridine are an order of magnitude less.

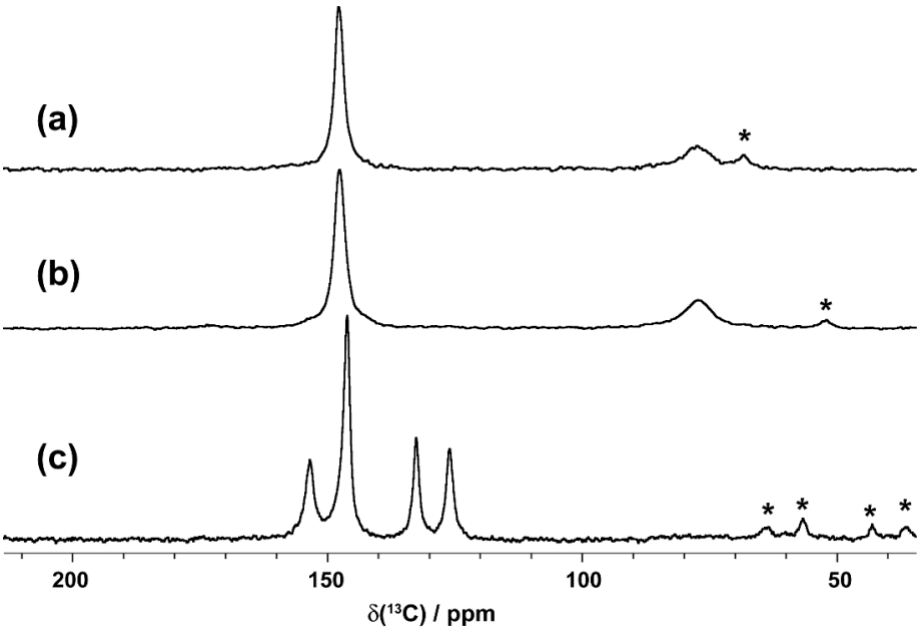

Figure 34. (a) ^{19}F→ ^{13}C CP/MAS NMR spectrum of solid p-diiodotetrafluorobenzene (ν_r = 10 kHz); (b) ^{19}F→ ^{13}C CP/MAS NMR spectrum of solid polymorph D (S0872) (ν_r = 12 kHz); (c) ^{1}H→ ^{13}C CP/MAS NMR spectrum of solid polymorph D (S0872) (ν_r = 11 kHz). A small halogen-bond induced chemical shift of 0.4 ppm is seen for the C-I carbons at ~77 ppm. Asterisks denote spinning sidebands.

The $^{19}F \rightarrow {}^{13}C$ CP/MAS and $^{1}H \rightarrow {}^{13}C$ CP/MAS NMR spectra of a powdered sample of cocrystal **C** are presented in **Figure 35 (b, c).** The $^{19}F \rightarrow {}^{13}C$ CP/MAS NMR spectrum of pure 1,4-diiodotetrafluorobenzene is also presented in **Figure 35(a).**

As is evident in **Figure 35 (b)**, the $^{19}F \rightarrow {}^{13}C$ CP/MAS experiment cleanly selects for those carbon atoms which are on the diiodotetrafluorobenzene ring, whereas the $^{1}H \rightarrow {}^{13}C$ CP/MAS NMR spectrum selects for those which are on the 3-nitropyridine molecule; this was also seen for cocrystal **D** (vide supra).

In comparison to the case of cocrystal **D**, slightly larger ^{13}C NMR frequency shifts are seen **Figure 35** upon formation of cocrystal **C**, relative to pure 1,4-diiodotetrafluorobenzene. The ^{13}C peaks for carbons directly bonded to fluorine show a decrease in average chemical shift of approximately 0.7 ppm upon cocrystallization whereas those bonded to iodine show an increase of approximately 1.6 ppm (**Table 10**). This seems to be opposite the general trend that a shorter halogen bond results in a larger increase in the C-I chemical shift[8,61]; however, the differences both in halogen bond length and ^{13}C chemical shifts when comparing cocrystals **C** and **D** are small.

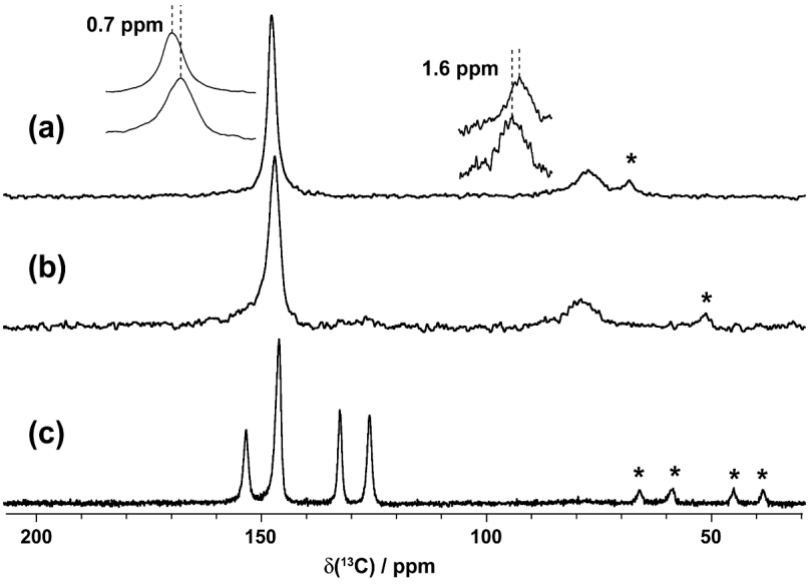

Figure 35.$^{19}F\rightarrow{}^{13}C$ CP/MAS NMR spectrum of solid *p*-diiodotetrafluorobenzene (ν_r = 10 kHz); (b) $^{19}F\rightarrow{}^{13}C$ CP/MAS NMR spectrum of solid polymorph **C** (S0790) (ν_r = 12 kHz); (c) $^{1}H\rightarrow{}^{13}C$ CP/MAS NMR spectrum of solid polymorph **C** (S0790) (ν_r = 11 kHz). A halogen-bond induced chemical shift of -0.7 ppm is seen for the C-F carbons at 147.6 ppm and of +1.6 ppm is seen for the C-I carbons at ~77 ppm. Asterisks denote spinning sidebands.

For cocrystal **B,** the $^{19}F\rightarrow{}^{13}C$ CP/MAS and $^{1}H\rightarrow{}^{13}C$ CP/MAS NMR spectra of a powdered sample of cocrystal **B** are presented in **Figure 36 (b, c).** The $^{19}F\rightarrow{}^{13}C$ CP/MAS NMR spectrum of pure 1,3,5-trifluoro-2,4,6-triiodobenzene (Szell et al., 2017) is also presented in **Figure 36 (a)** for comparison purposes.

In **Figure 36 (b)**, the $^{19}F\rightarrow{}^{13}C$ CP/MAS experiment cleanly selects for those carbon atoms which are on the 1,3,5-trifluoro-2,4,6-triiodobenzene. In addition to the dominant aromatic C-F resonances at ~163 ppm, a weaker and a little broader peak at ~ 75 ppm,

another peak at ~66 ppm that is attributed to the carbons directly bonded to iodine (see **Table 10**). The halogen bond formed between I1 and N1.

Carbon-13 CP/MAS SSNMR spectroscopy was carried out on all samples to characterize both the halogen-bond donor and the halogen-bond acceptor in terms of their ^{13}C chemical shifts. $^{1}H \rightarrow {}^{13}C$ CP proved to be an effective method in characterizing the halogen-bond acceptor because of the protons covalently bonded to the acceptor moieties (see **Figure 36**).

The chemical shifts of the carbons covalently bonded to nitrogen on the halogen-bond acceptor are listed in **Table 10**.

Across all the spectra, a ^{13}C chemical shift change for the carbons covalently bonded to nitrogen on the halogen-bond acceptor is observed when the starting material is compared to the halogen-bonded cocrystals.

In comparison to the case of cocrystal **B**, slightly larger ^{13}C NMR frequency shifts are seen in **Figure 36** upon formation of cocrystal **B**, relative to pure 1,3,5-trifluoro-2,4,6-triiodobenzene. The ^{13}C peaks for carbons directly bonded to fluorine show an increase in average chemical shift of approximately 0.4 ppm upon cocrystallization whereas those bonded to iodine show a decrease of approximately 1.2 ppm (**Table 10**).

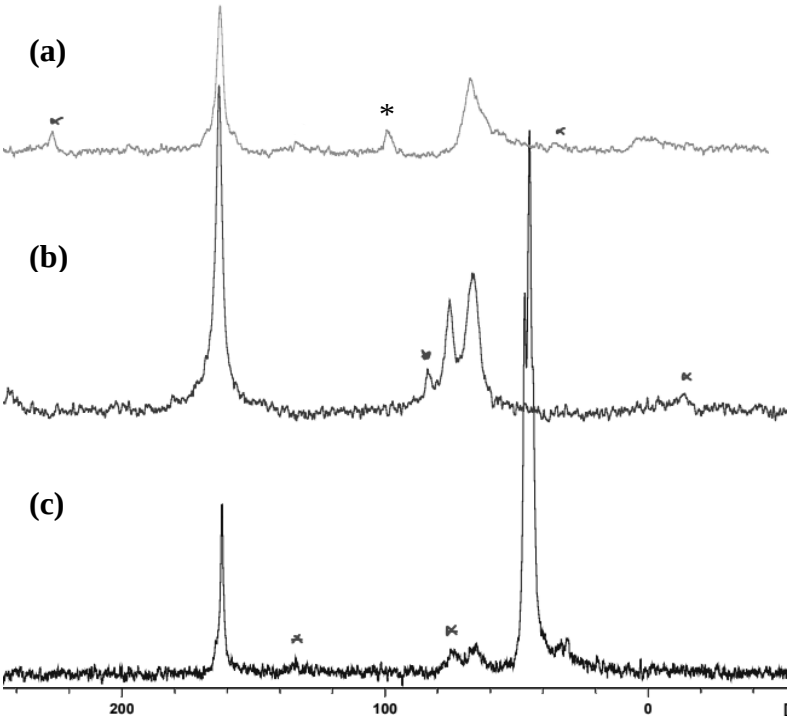

Figure 36.$^{19}F\rightarrow{}^{13}C$ CP/MAS NMR spectrum of solid 1,3,5-trifluoro-2,4,6-triiodobenzene (ν_r = 8 kHz); (b) $^{19}F\rightarrow{}^{13}C$ CP/MAS NMR spectrum of solid cocrystal (S0854) (ν_r = 10 kHz); (c) $^{1}H\rightarrow{}^{13}C$ CP/MAS NMR spectrum of solid cocrystal B (S0854) (ν_r = 9 kHz). Asterisks denote spinning sidebands.

The large number of crystallographically distinct C-I···N halogen bonds (twelve) in the three stoichiometric cocrystals studied here provides an interesting opportunity to assess the relationship between halogen bond distance and angle maintaining the same nominal chemical composition. However, even under these controlled conditions, no strong correlation was observed **(Figure 37).** In **Figure 38** some photos of cocrystals obtained while working in the laboratory and the cocrystallization method used (slow evaporation).

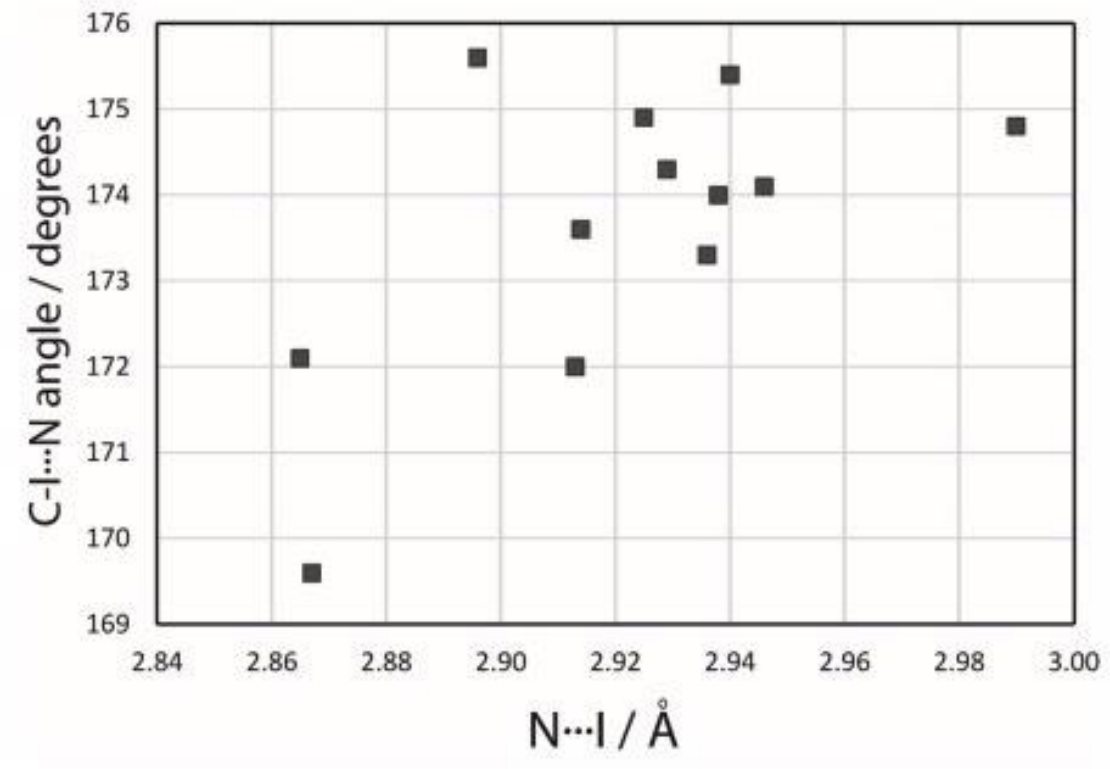

Figure 37. Lack of correlation between nitrogen-iodine halogen bond distances and angles in stoichiometric cocrystals A, C, and D (Hajjar et al., n.d.).

Table 10. Carbon-13 Isotropic Chemical Shifts Measured in the Solid State.

	$^{1}H \rightarrow {}^{13}C$ CP/MAS	$^{19}F \rightarrow {}^{13}C$ CP/MAS*
p-diiodotetrafluorobenzene	n/a	147.6 ± 0.3, 76.8 ± 1.4
1,3,5-trifluoro-2,4,6-triiodobenzene*	n/a	162.6± 0.9, 67.6± 2.4
cocrystal **B**	45.0748±0.2,47.1237± 0.2,162.2011± 0.2	163.0443±0.2,75.0732± 0.2,66.4745± 0.2
cocrystal **C**	125.9 ± 0.2, 132.6 ± 0.2, 146.1 ± 0.2, 153.4 ± 0.2	147.1 ± 0.3, 78.4 ± 1.5
cocrystal **D**	125.9 ± 0.2, 132.5 ± 0.2, 146.0 ± 0.2, 153.3 ± 0.2	147.6 ± 0.3, 77.2 ± 1.5

*****For carbons bonded to iodine, these are peak positions and are thus only the approximate true isotropic chemical shifts due to residual dipolar coupling between ^{13}C and ^{127}I. The peak positions are clearly different for different samples (see e.g., Figure 35); However, large errors are assigned due to uncertainty in the quantitative effects of the residual dipolar coupling on the peak positions. Errors on other chemical shifts for carbons not bonded to iodine reflect the reproducibility of the measurement.

*The spectrum of 1,3,5-trifluoro-2,4,6-triiodobenzene data collection is taken from reference 8 (Szell et al., 2017).

Table 11. Key Geometric Descriptors of Halogen Bonds in the Stoichiomorphs.

Cocrystal	$r_{N\cdots I}$ / Å	C-I ···N angle
B	2.82	178°
C	2.940; 3.036[a]	175.4°; 177.5°[a]
D	2.896	175.6°
A (site 1)	2.913	172.0°
A (site 2)	2.925	174.9°
A (site 3)	2.867	169.6°
A (site 4)	2.946	174.1°
A (site 5)	2.936	173.3°
A (site 6)	2.938	174.0°
A (site 7)	2.990	174.8°
A (site 8)	2.914	173.6°
A (site 9)	2.865	172.1°
A (site 10)	2.929	174.3°

O···I halogen bond.

Table 12. Hydrogen-bond geometry (Å, ° for S0854).

D—H···A	D—H	H···A	D···A	D—H···A
N1—H1···I2i	0.86 (2)	3.12 (2)	3.978 (3)	177 (3)
C7—H7A···F2ii	0.98	2.40	3.299 (4)	152
C7—H7AB···I3iii	0.98	3.23	3.990 (3)	135
C8—H8A···I2iv	0.98	3.19	4.001 (3)	141
C8—H8AB···I1v	0.98	3.26	3.879 (3)	123

Figure 38. Different techniques of cocrystallization and some photos of cocrystals.

Chapter 6: Conclusions

6.1 General conclusion

Three novel stoichiometric cocrystals of 1,4-diiodotetrafluorobenzene and 3-nitropyridine with molar ratios of 1:1, 2:1, and 1:2, and the cocrystal of piperazine and 1,3,5-trifluoro-2,4,6-triiodobenzene with molar ratio 2:1, have been prepared by slow evaporation method and characterized by single-crystal X-ray diffraction, powder-X-ray diffraction, and $^{19}F \rightarrow {}^{13}C$ CP/MAS and $^{1}H \rightarrow {}^{13}C$ CP/MAS NMR spectroscopy.

Let's start with the three stoichiomorphs. Each pack in a different space group and they all feature halogen bonds between iodine and the pyridyl ring nitrogen. In only one case is a halogen bond between iodine and an oxygen atom on the nitro group observed. Ten crystallographically distinct halogen bonds are observed in the 1:2 cocrystal. Thus, significant crystallographic differences are seen for a set of three chemically identical (with varying stoichiometry) systems.

^{13}C solid-state NMR spectroscopy showed small frequency shifts of the C-I peak of 1,4-diiodotetrafluorobenzene upon halogen bond formation, and cross-polarization from ^{19}F to ^{13}C vs ^{1}H to ^{13}C provided clean spectral editing, with the former experiment generating a subspectrum of the fluorinated halogen bond donor and the latter generating a subspectrum of the halogen bond acceptor.

Cocrystallization of the low-melting 3-nitropyridine provided a route to maintain this component in the solid state over a larger temperature range. For the cocrystal of piperazine and 1,3,5-trifluoro-2,4,6-triiodobenzene, features a moderately strong halogen bond between one of the three crystallographically distinct iodine atoms and the nitrogen atom.

Overall, this work contributes to the systematic exploration of the polymorphic and stoichiometric cocrystal landscape of halogen-bonded systems.

6.2 Future work

Another work that can be done it would be to reuse the halogen bond donors (1,4-diiodotetrafluorobenzene and 1,3,5-trifluoro-2,4,6-triiodobenzene) and make them cocrystallize with a series of acceptors containing nitrogen using the mechanochemistry techniques and slow evaporation method and evaluate the electrostatic interactions with different techniques such as SCXRD and SSNMR.

References

1. Aakeröy, C.; Sinha, A. S. Co-crystals: Preparation, Characterization and Applications. Aakeröy, C. B. and Sinha, A. S., Eds. *Royal Society of Chemistry*. **2018**,*24*.

2. Salzillo, T.; Masino, M.; Kociok-Köhn, G.; Di Nuzzo, D.; Venuti, E.; Della Valle, R. G.; Vanossi, D.; Fontanesi, C.; Girlando, A.; Brillante, A.; Da Como, E. *Cryst. Growth. Des.* **2016**, *16*, 3028-3036.

3. Cinčić, D.; Friščić, T.; Jones, W. *J. Am. Chem. Soc.* **2008**, *130*, 7524-7525.

4. Desiraju, G. R.; Ho, P. S.; Kloo, L.; Legon, A. C.; Marquardt, R.; Metrangolo, P.; Politzer, P.; Resnati, G.; Rissanen, K. *Pure Appl. Chem.* **2013**, *85*, 1711-1713.

5. Lisac, K.; Topić, F.; Arhangelskis, M.; Halogen-bonded cocrystallization with phosphorus, arsenic and antimony acceptors. *Nat Commun.***2019,***10***.**

6. Gilday, L. C.; Robinson, S. W.; Barendt, T. A.; Langton, M. J.; Mullaney, B. R.; Beer, P. D. *Chem. Rev.* **2015**, *115*, 7118-7195.

7. Cavallo, G.; Metrangolo, P.; Milani, R.; Pilati, T.; Priimagi, A.; Resnati, G.; Terraneo, G. *Chem. Rev.* **2016**, *116*, 2478-2601.

8. Szell, P. M. J.; Gabriel, S. A.; Gill, R. D. D.; Wan, S. Y. H.; Gabidullin, B.; Bryce, D. L. *Acta Cryst.* **2017**, *C73*, 157-167.

9. Szell, P. M. J.; Dragon, J.; Zablotny, S.; Harrigan, S. R.; Gabidullin, B.; Bryce, D. L. *New. J. Chem.* **2018**, *42*, 10493-10501.

10. Morin, V. M.; Szell, P. M. J.; Caron-Poulin, E.; Gabidullin, B.; Bryce, D. L. *ChemistryOpen* **2019**, *8*, 1328-1336.

11. Aitipamula, S. et al. *Cryst. Growth Des.* **2012**, *12*, 2147-2152.

12. Trask, A. V. *Mol. Pharm.* **2007**, *4*, 301-309.

13. Raza, K.; Kumar, P.; Ratan, S.; Malik, R.; Arora, S. Polymorphism: The Phenomenon Affecting the Performance of Drugs. *SOJ Pharm Pharm Sci.* **2014,** *1,* 10.

14. Gosar, D. A.; Hussain, D. S.; Shaikh, D. T. Polymorphism and polymorph characterisation in pharmaceuticals. *Journal of Biomedical and Pharmaceutical Research*. **2019**, *8*.

15. Karimi-Jafari, M.; Padrela, L.; Walker, G.; Croker, D. Creating Cocrystals: A Review of Pharmaceutical Cocrystal Preparation Routes and Applications. *Crystal Growth & Design*. **2018,** *18*, 6370-6387.

16. Levitt, M. H. *Spin Dynamics: Basics of Nuclear Magnetic Resonance*, 2nd ed.; John Wiley & Sons Ltd.: West Sussex, **2008**.

17. Domagała, M.; Matczak, P.; Palusiak, M. Halogen bond, hydrogen bond and N···C interaction – On interrelation among these three noncovalent interactions. *Computational and Theoretical Chemistry*. **2012**, *998*, 26–33.

18. Rovnyak, D. Tutorial on analytic theory for cross-polarization in solid state NMR. *Concepts in Magnetic Resonance Part A.* **2008,** *32A*, 254–276.

19. Alia, A.; Ganapathy, S.; de Groot, H. Magic angle spinning (MAS) NMR: a new tool to study the spatial and electronic structure of photosynthetic complexes. *Photosynthesis Research*. **2009,***102,* 415-425.

20. Bondi, A. *J. Phys. Chem.* **1964**, *68*, 441-451.

21. Steiner, T. The Hydrogen Bond in the Solid State. *Angew. Chem. Int. Ed.* **2002**, *41*, 48-76.

22. Southern, S. Investigations of Non-Covalent Carbon Tetrel Bonds by Computational Chemistry and Solid-State NMR Spectroscopy. **2016.** [Doctoral thesis, University of Ottawa].

23. Brinck, T.; Murray, J. S.; Politzer, P. Surface Electrostatic Potentials of Halogenated Methanes as Indicators of Directional Intermolecular Interactions. *Int. J. Quantum Chem*. **1992**, *19*, 57-64.

24. Clark, T.; Hennemann, M.; Murray, J. S.; Politzer, P. Halogen bonding: the sigma-hole. Proceedings of "Modeling interactions in biomolecules II", Prague, September 5th-9th, 2005. *J. Mol. Model.* **2006**, *13*, 291-296.

25. Ding, X.; Tuikka, M.; Haukk, M. Halogen Bonding in Crystal Engineering. *Recent Advances in Crystallography*. **2012b**.

26. Alkorta, I.; Blanco, F.; Solimannejad, M.; Elguero, J. Competition of Hydrogen Bonds and Halogen Bonds in Complexes of Hypohalous Acids with Nitrogenated Bases. *The Journal of Physical Chemistry A.* **2008,** *112* (43).

27. Von, P.; Schleyer, R.; and West, R. *J. Am. Chem. Soc.* **1959**, *81*, 3164–3165.

28. Colin, M. M.; Gaultier de Claubry, H. Sur Le Combinaisons de L'iode Avec Les Substances Végétales et Animales. *Ann. Chim*. **1814**, *90*, 87−100.

29. Pelletier, P.; Caventou, J. Sur Un Nouvel Alcali Végétal (la Strychine) Trouvé Dans La Fève de Saint-Ignace, La Noix Vomique Etc. *Ann. Chim. Phys*. **1819**, *10*, 142−177.

30. Svensson, P. H.; Kloo, L. Synthesis, Structure, and Bonding in polyiodide and Metal Iodide-Iodine Systems. *Chem. Rev*. **2003**, *103*,1649−1684.

31. Jörgensen, S. M. Ueber Einige Anorganische Superjodide. *J. Prakt. Chem*. **1870**, *2*, 347−360.

32. Remsen, I.; Norris, J. F. Action of the Halogens on the methylamines. *Am. Chem. J.* **1896**, *18*, 90−95.

33. Ault, B. S.; Andrews, L. Infrared and Raman Spectra of the M^+F3^- ion Pairs and their mixed Chlorine-Fluorine Counterparts in solid Argon. *Inorg. Chem*. **1977**, *16*, 2024−2028.

34. Ault, B. S.; Andrews, L. Matrix Reactions of Alkali Metal Fluoride Molecules with Fluorine. Infrared and Raman Spectra of the Trifluoride Ion in the M^+F3^- Species. *J. Am. Chem. Soc*. **1976**, *98*,1591−1593.

35. Riedel, S.; Köchner, T.; Wang, X.; Andrews, L. Polyfluoride Anions, a Matrix-Isolation and Quantum-Chemical Investigation.*Inorg. Chem***. 2010**, *49*, 7156−7164.

36. Legon, A. C. Prereactive Complexes of Dihalogens XY with Lewis Bases B in the Gas Phase: A Systematic Case for the Halogen Analogue B···XY of the Hydrogen Bond B···HX. *Angew. Chem., Int*. Ed.1**999**, *38*, 2686−2714.

37. Cardillo, P.; Corradi, E.; Lunghi, A.; Meille, S. V.; Messina, M. T.; Metrangolo, P.; Resnati, G. The N···I Intermolecular Interaction as a General Protocol for the Formation of Perfluorocarbon-Hydrocarbon Supramolecular Architectures. Tetrahedron. **2000**, *56*, 5535−5550.

38. Metrangolo, P.; Murray, J. S.; Pilati, T.; Politzer, P.; Resnati, G.; Terraneo, G. Fluorine-Centered Halogen Bonding: A Factor in Recognition Phenomena and Reactivity. *Cryst. Growth Des*. **2011**, *11*,4238−4246.

39. Cametti, M.; Crousse, B.; Metrangolo, P.; Milani, R.; Resnati, G. The Fluorous Effect in Biomolecular Applications. *Chem. Soc. Rev*.**2012**, *41*, 31−42.

40. Pavan, M. S.; Durga Prasad, K.; Row, T. N. G. Halogen Bonding in Fluorine: Experimental Charge Density Study on Intermolecular F···F and F···S Donor-Acceptor Contacts. *Chem. Commun*. **2013**, *49*,7558−7560.
41. Schwerdtfeger, P. Atomic Static Dipole Polarizabilities. In Atoms, Molecules and Clusters in Electric Fields; Maroulis, G., Ed.; *Imperial College Press*. **2006**,1−32.
42. Shannon, R.D. *Acta Crystallogr*. **1976**, *Sect. A, 32*, 751–767.
43. Alvarez, S. *Dalton Trans* .**2013,** *42*, 8617.
44. Metrangolo, P., Meyer, F., Pilati, T. et al. Angew. Chem. Int. Ed. **2008,** *47*: 6114–6127.
45. Priimagi, A.; Cavallo, G.; Metrangolo, P.; and Resnati, G. *Acc. Chem. Res.* **2013,** *46*, 2686–2695.
46. Riel, A.M.S.; Jessop, M.J.; Decato, D.A. et al. *Acta Crystallogr. Sect. B Struct. Sci. Cryst. Eng. Mater*. **2017,** *73*, 203–209.
47. Van de Streek, J.; Motherwell, S. Searching the Cambridge Structural Database for polymorphs. *Acta Crystallographica Section B Structural Science*. **2005,** *61*, 504-510.
48. Cheng, L.; Zhu, B.; Ma, X.; Zhang, Z.; Wang, J.; Zhang, Q.; Mei, X. Identification of an Overlooked Halogen-Bond Synthon and Its Application in Designing Fluorescent Materials. *Chemistry – A European Journal*. **2019,** *25*, 6584-6590.
49. Xu, Y.; Viger-Gravel, J.; Korobkov, I.; Bryce, D. Mechanochemical Production of Halogen-Bonded Solids Featuring P═O···I–C Motifs and Characterization via X-ray Diffraction, Solid-State Multinuclear Magnetic Resonance, and Density Functional Theory. *The Journal of Physical Chemistry C*. **2015,** *119*, 27104-27117.

50. Kobra, K.; O'Donnell, S.; Ferrari, A.; McMillen, C.; Pennington, W. New Journal of Chemistry. **2018**, *42*, 10518-10528.
51. Szell, P. M. J., Gabriel, S. A., Caron-Poulin, E., Jeannin, O., Fourmigué, M., & Bryce, D. L. *Crystal Growth & Design*. **2018,***18*.
52. Widdifield, C. M.; Cavallo, G.; Facey, G. A.; Pilati, T.; Lin, J.; Metrangolo, P.; Resnati, G.; Bryce, D. L. *Chem. Eur. J.* **2013**, *19*, 11949-11962.
53. APEX Softward Suite v 2010 Bruker AXS Inc. Madison Wisconsin USA, **2010**.
54. Blessing, R. H. *Acta Crystallogr. Sect. A* **1995**, *51*, 33–38.
55. Sheldrick, G. M. *Acta Crystallogr. A.* **2008**, *64*, 112–22.
56. Hübschle, C. B.; Sheldrick, G. M.; Dittrich, B. *J. Appl. Crystallogr.* **2011**, *44*, 1281–1284.
57. Kaupp, M. Relativistic Effects on NMR Chemical Shifts, Chapter 9 in Relativistic Electronic Structure Theory: Part 2. Applications. Schwerdtfeger, P., Ed.: **2004**, *14.*
58. Pyykkö, P.; Görling, A.; Rösch, N. *Mol. Phys*. **1987**, *61*, 195-205.
59. Kaupp, M.; Malkina, O. L.; Malkin, V. G.; Pyykkö. P. *Chem. Eur. J.* **1998**, *4*, 118-126.
60. Vicha, J.; Švec, P.; Růžičková, Z.; Samsonov, M. A.; Bártová, K.; Růžička, A.; Straka, M.; Dračinskỳ, M. *Chem. Eur. J.* **2020**, *26*, 8698-8702.
61. Viger-Gravel, J.; Leclerc, S.; Korobkov, I.; Bryce, D. L. *CrystEngComm* **2013**, *15*, 3168-3177.
62. Cameron F. Holder and Raymond E. Schaak ACS Nano. **2019**,*13*, 7359-7365.
63. Lee, E. A practical guide to pharmaceutical polymorph screening & selection. *Asian Journal of Pharmaceutical Sciences*. **2014**, *9*, 163-175.

64. Rissanen, K. Halogen bonded supramolecular complexes and networks. *Crystengcomm*. **2008,** *10*, 1107.

65. Kolodziejski, W.; Klinowski, J. Kinetics of Cross-Polarization in Solid-State NMR: A Guide for Chemists. *Chemical Reviews*. **2002,***102*, 613-628.

66. Hajjar, C.; Ovens, J.; Bryce, D. 1,3,5-Trifluoro-2,4,6-triiodobenzene–piperazine (2/1). *Iucrdata*. **2021,***6* (10).

67. Hajjar, C.; Nag, T.; Al Sayed, H.; Ovens, J.;Bryce, D. Stoichiomorphic Halogen-Bonded Cocrystals. A Case Study of 1,4-Diiodotetrafluorobenzene and 3-Nitropyridine. *Canadian Journal Of Chemistry.***2021.**